Effect of Fuel Properties on First Cycle Fuel Delivery In a Port Fuel Injected Spark Ignition Engine

by

Kevin R. Lang

S.B., Mechanical Engineering
Massachusetts Institute of Technology, 2002

SUBMITTED TO THE DEPARTMENT OF MECHANICAL ENGINEERING
IN PARTIAL FULFULLMENT OF THE REQUIREMENTS FOR THE DEGREE OF

MASTER OF SCIENCE IN MECHANICAL ENGINEERING
AT THE
MASSACHUSETTS INSTITUTE OF TECHNOLOGY

JUNE 2004

Signature of Author. _____
Department of Mechanical Engineering
May 7, 2004

Certified by: _____
Wai K. Cheng
Professor of Mechanical Engineering
Thesis Supervisor

Accepted by: _____
Ain A. Sonin
Chairman, Departmental Graduate Committee

Effect of Fuel Properties on First Cycle Fuel Delivery In a Port Fuel Injected Spark Ignition Engine

by

Kevin R. Lang

Submitted to the Department of Mechanical Engineering
on May 7, 2004 in Partial Fulfillment of the
Requirements for the Degree of Master of Science in
Mechanical Engineering

ABSTRACT

Achieving robust combustion while also yielding low hydrocarbon (HC) emissions is difficult for the first cycle of cranking during the cold start of a Port Fuel Injected (PFI) Spark Ignition (SI) engine. Cold intake port wall and valve temperatures, near-atmospheric manifold pressure, and low port air velocity combine to create an adverse environment for fuel delivery – the process of injecting and vaporizing liquid fuel to create a combustible air-fuel mixture. As a result, only a small fraction of the injected fuel mass contributes to the combustible mixture; the fraction is less than 10% at cold ambient temperatures.

With fast light off catalysts, the first cycle produces a significant portion of the total trip emissions. The low fuel delivery fraction results in high residual liquid fuel in both the port and cylinder; this fuel contributes significantly to the exhaust HC emissions. Since the first cycle engine control is open-loop, the Engine Control Unit (ECU) must determine how much fuel to inject under given conditions – temperature, pressure, and for a given fuel. Fuel properties play a significant role in first cycle fuel delivery, since the energy available for vaporization is a limiting factor in fuel delivery.

The effect of fuel properties on fuel delivery for the first cycle was quantified at a wide range of cold start temperatures by using a skip-firing strategy to simulate the first cycle of cranking on a production PFI engine. Four fuels between 1083 and 1257 Driveability Index (DI) were tested, and the fuel delivery results have been correlated to properties of the ASTM distillation curve. The fractional distillation point that correlates to fuel delivery is a function of temperature – at colder temperatures, the results correlate with the more volatile end of the distillation curve.

Fuel delivery results for the fuels were also simulated with a thermodynamics-based fuel delivery model based on partial equilibrium with the charge air.

Thesis Supervisor: Wai K. Cheng
Title: Professor of Mechanical Engineering

Acknowledgements

I am grateful to many people in the Sloan Automotive Laboratory for their help over the past two years, but several individuals deserve particular recognition.

I owe a great debt of gratitude to Prof. Wai K. Cheng for his help and guidance throughout this project. He was always available and glad to help when things went wrong with testing, and his patience, knowledge, and understanding were greatly appreciated. I look forward to continuing my research with him over the next few years.

Thane DeWitt has been an invaluable resource in the lab, always ready to help me with the daily emergencies of research. I am not the only student in the lab to whom Thane must attend, but he is a master juggler and has always shown as much concern for my research as I have.

I have greatly enjoyed my time thus far in the Sloan Lab thanks largely to my fellow students, who help to make this an exceptionally fun and friendly place to work. I would like to thank Halim Santoso for his help and guidance with my research; he laid the foundation for my research with his own project, and much of what I have accomplished built off of his hard work. Brian Hallgren's years of experience and expertise have been a huge asset, and he will be sorely missed when he graduates some day. I would also like to thank Tony Zhang, Jeff Matthews, Jeremy Llaniguez, and Ioannis Kitsopanidis for their help with various aspects of my research.

This research was generously supported by the Engine and Fuels Research Consortium, which includes DaimlerChrysler, Ford Motor Company, General Motors, Delphi, and Saudi Aramco. I must especially thank former consortium member ExxonMobil, and Yeong Kwon in particular. Without their help and support with providing test fuels and the supporting data, this project would not have been possible.

I am eternally grateful to my parents for their continued love and support. Without them I would never have made it to MIT in the first place. I would like to thank my father for helping to instill my love for cars at a young age, without which I might never have ended up an engineer. I would also like to thank my mother for her understanding as research keeps me away from home more than I would like.

Finally, I must thank my girlfriend, Patricia Young, for her patience and support throughout my time in graduate school thus far. If not for you I might not be here at all, but there is no place else I would rather be. My life is infinitely better for having you share it with me.

TABLE OF CONTENTS

LIST OF FIGURES & TABLES

LIST OF FIGURES

LIST OF TABLES

NOMENCLENTURE

AFR	Air Fuel Ratio
ABDC	After Bottom Dead Center
ATDC	After Top Dead Center
BDC	Bottom Dead Center
BTDC	Before Top Dead Center
CAD	Crank Angle Degrees
CP	Constant Pressure
DI	Driveability Index
ECT	Engine Coolant Temperature
ECU	Engine Control Unit
FFID	Fast Flame Ionization Detector
HC	Hydrocarbon
HSM	Hydrocarbon Sampling Module
IVC	Intake Valve Closing
IVO	Intake Valve Opening
LHC	Line Heater Controller
MAP	Manifold Absolute Pressure
MCU	Main Control Unit
MTBE	Methyl Tertiary Butyl Ether
PDF	Probability Density Function
PFI	Port Fuel Injected
RPM	Revolutions Per Minute
RVP	Reid Vapor Pressure
SI	Spark Ignition
SSP	Sampling Spark Plug
TDC	Top Dead Center
T10	10% ASTM Distillation Temperature
T50	50% ASTM Distillation Temperature
T90	90% ASTM Distillation Temperature

m_a	Mass of air
m_f	Mass of fuel
M_a	Molecular weight of air
M_f	Molecular weight of fuel
n_a	Moles of air
n_f	Moles of fuel
R_a	Gas constant for air
T_a	Air temperature
X_f	Fuel mass fraction
Y_f	Fuel mole fraction

Φ	Phi, fuel air equivalence ratio

Chapter 1

INTRODUCTION

1.1 Background

The advent of fast light off catalysts has dramatically reduced tailpipe emissions of unburned hydrocarbons (HC) from vehicles with spark ignition (SI) engines. However, even fast light off catalysts do not reach their operating temperature, about 250°C, until a few seconds of engine operation. During these few seconds after the engine is started, any HC emissions leaving the engine are exhausted to the atmosphere.

While the catalyst warms up very quickly, the engine itself warms up on a much longer time scale, typically several minutes. In port fuel injected (PFI) engines, the fuel is injected toward the back of the intake valve, so that during normal engine operation the liquid fuel vaporizes quickly due to heating from the valve. When the engine is cold, however, vaporizing the fuel becomes much more difficult, and thus excess liquid fuel must be injected in order to yield a combustible air-fuel mixture. Since the residual fuel is a significant source of HC emissions, this practice results in very high HC emissions until the catalyst reaches its operating temperature.

Achieving robust combustion for the first cycle of cranking is crucial to fast, reliable engine startup. However, doing so while also yielding low HC emissions is difficult due to several conditions which adversely affect fuel delivery. First, liquid fuel is injected onto the cold intake port wall and valve. Second, for the first cycle, the intake manifold is at or near atmospheric pressure, since the intake manifold volume is much greater than the engine displacement volume. This relatively high pressure limits the evaporation of liquid fuel relative to steady state idling. Finally, since the engine cranking speed is typically only 200-300 RPM, air velocities in the intake port are relatively low, thus yielding low convective mass transfer. As a result, only a small fraction of the injected fuel mass enters the combustible mixture, sometimes less than 10% at cold ambient temperatures. Since so little of the injected fuel mass enters the combustible mixture, a substantial amount remains as liquid fuel. Some fraction of this residual fuel will subsequently leave the engine as HC emissions.

Under normal operating conditions, the engine is controlled by feedback from an oxygen sensor to the Engine Control Unit (ECU). The oxygen sensor effectively monitors the air-fuel ratio, and adjusts the injected mass of fuel in order to maintain a stoichiometric mixture. During cranking, however, engine control is open loop, and the ECU must predict how much fuel to inject for the given conditions. To ensure a robust startup under a variety of conditions and allowing for differences in consumer fuels, engine calibrations are generally very conservative and inject more than enough fuel to start the engine. This results in higher HC emissions.

Currently, engine calibrations account for changes in ambient temperature when determining the fuel injection pulse width for the first cycle, since colder temperatures negatively impact fuel delivery. Another major factor which is not currently accounted for is fuel properties. Different fuels can have dramatically different fuel delivery behaviors, to the extent that, for a given injected mass, one fuel might yield a combustible mixture, while another fuel might not. If fuel delivery behavior could be correlated to fuel properties, the optimal injected mass – that which yields a robust, combustible mixture and minimized HC emissions – could be determined for a given fuel.

1.2 Previous Works

To date, limited research into fuel delivery during cranking has been conducted. This is largely due to the fact that fast light off catalysts are a relatively recent development, and thus emissions during the cranking process has become critical only recently. Past work has sought to visualize fuel transport for the first cycle [1], determine the minimum injected fuel mass required for combustion during cranking [2], and measure in-cylinder mixture composition [3]. While these studies gave insight into the cranking process, they did not look at the impact of fuel properties.

The first cycle of cranking represents the most difficult environment for fuel delivery of the entire cranking and cold start process, but results from cold start driveability studies still indicate some of the general trends driven by fuel properties. Several studies found that the 50% distillation temperature (T50) and/or Driveability Index (DI)[1] are significant indicators of cold start performance. [2] [4] [5] [6] Additionally, the low- to mid-range volatility fuel components

[1] DI is an industry standard indication of fuel volatility. It is defined based on test points on the ASTM distillation curve, the Fahrenheit temperatures at which 10%, 50%, and 90% of the fuel has vaporized. These are known as T10, T50, and T90. DI = 1.5*T10 + 3*T50 + T90.

were found to impact driveability. [7] [4] Another commonly reported fuel property, Reid Vapor Pressure (RVP), was found to be insignificant. [8] [4] Additionally, oxygenated fuels, containing Methyl Tertiary Butyl Ether (MTBE), have different correlations than non-oxygenated fuels. [9] [4]

These studies did not look specifically at the first cycle of cranking, however. One study determined the minimum amount of fuel needed to yield a combustible mixture for each of the first three cycles, for three different fuels. Fuels with higher T50 required more injected mass to achieve a combustible mixture, i.e. a smaller fraction of the fuel is delivered to the charge at T50 increases. [2] However, this testing was not conducted over a range of temperatures, and no direct correlation to T50 was established. The conclusions regarding fuel effects were qualitative only. Nonetheless, these results did show that different fuels can exhibit markedly different fuel delivery behavior during cranking, thus demonstrating the potential for correlating fuel delivery to quantifiable fuel properties.

1.3 Objective

Through their effect on fuel delivery, fuel properties cascade to critical startup metrics such as residual fuel, combustion quality, and HC emissions. This study, however, focuses solely on fuel delivery, specifically the fraction of the injected fuel mass that mixes with air to form a combustible mixture. By determining this fraction as a function of injected mass, temperature, and fuel properties, a calibration scheme could be devised to ensure a robust, combustible mixture without overfueling and thus yielding higher than necessary HC emissions.

This research seeks to establish trends that could be broadly applied in engine development. The objective is not to directly reduce HC emissions, but to provide useful results and understanding of fuel property effects on fuel delivery, such that first cycle fueling could be optimized during engine development. As such, the fuel properties investigated are those commonly available to the calibration engineer – the ASTM distillation curve, DI, and RVP.

1.4 Methodology

Figure 1.1 shows the engine speed, cylinder pressure, Manifold Absolute Pressure (MAP), and fuel pulse width for a normal engine start. In normal engine operation, the engine is cranked by an electric starter motor, typically yielding cranking speeds between 200 and 300

RPM. The MAP drops slowly during cranking due to the large volume of the intake manifold relative to the engine displacement volume. Once the ECU senses crankshaft rotation, it synchronizes with the camshaft position sensor to determine engine timing, and then injects a large mass of fuel to each cylinder simultaneously. As such, the injection timing relative to engine position is different for each cylinder, and will thus be more favorable for combustion in some cylinders than others. Over-fueling all cylinders is necessary to ensure that at least once cylinder will fire on the first cycle. After this initial fuel injection event, injection occurs sequentially for each cylinder.

In the real world, however, the startup process is not perfectly repeatable because the engine shutdown process is uncontrolled. Depending on the engine cycle position from shutdown and which cylinders did not achieve combustion before the engine stopped, the cranking process can vary substantially. [10] [11]

To study the first cycle of cranking in a repeatable, controllable method, the starter motor was previously replaced by a pulley system coupled to a motoring dynamometer, to provide low-speed engine control. MAP was controlled using a throttle valve to yield values comparable to cranking at the same RPM in a normal engine. Figure 1.2 shows the correlation between MAP and cranking speed. [12] To achieve a repeatable starting condition for the first injection event, the engine was operated in a skip firing mode, where fuel is injected for a single cycle and then injection is skipped for many cycles. See Figure 1.3 for a typical pressure trace from skip firing. This allows air flowing through the engine to purge the residual fuel from the intake port and cylinder, until the engine is dry. Once this state is achieved, fuel is injected once again, and the skip firing process repeats. Thus the first cycle of cranking can be simulated in a readily repeatable manner without a full warm-up and shutdown process, which can take several hours.

Figure 1.1 – Cranking Behavior for Ford Zetec 4-Cylinder Engine

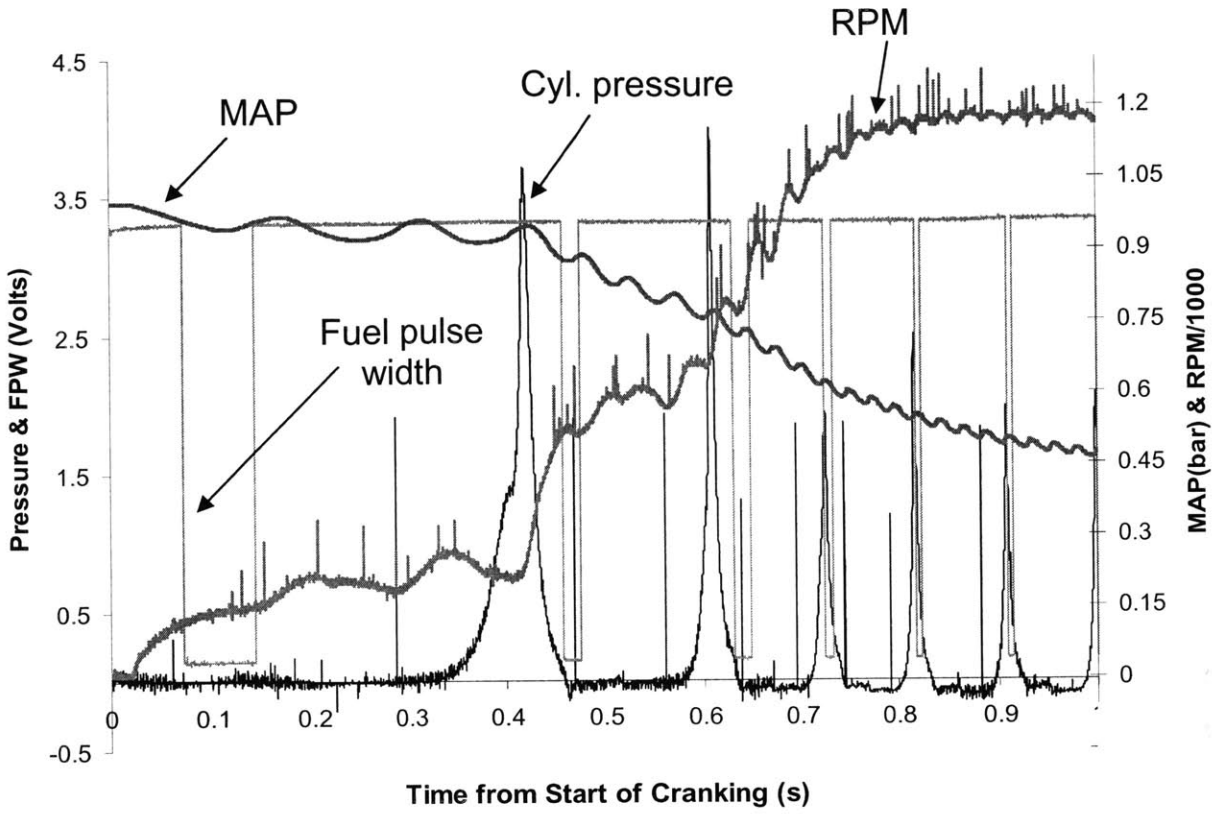

Figure 1.2 – MAP vs. Cranking Speed

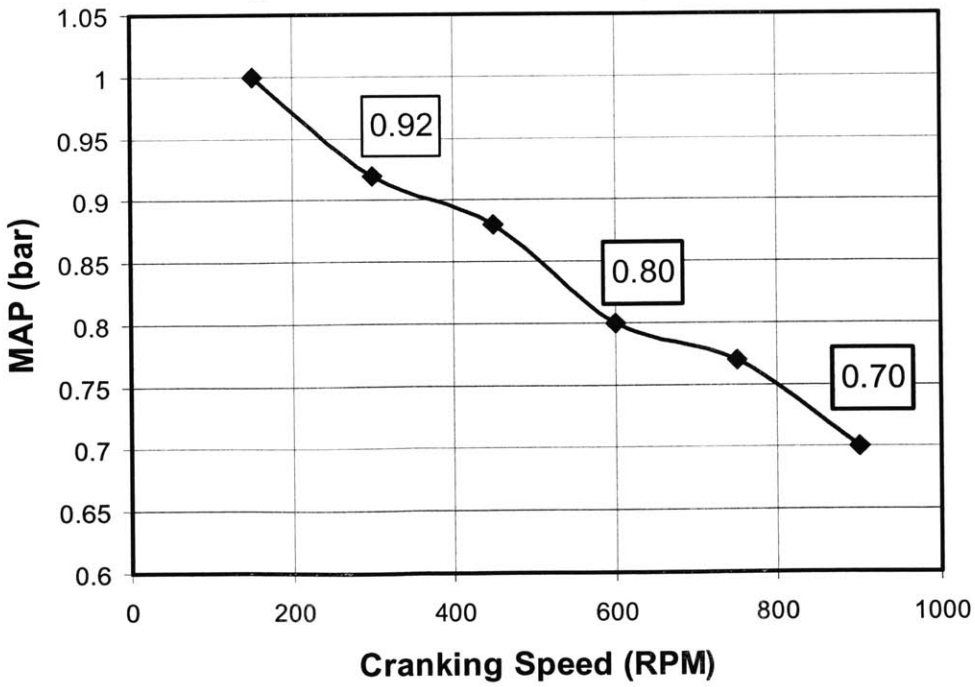

Figure 1.3 – Pressure Trace for Skip Firing

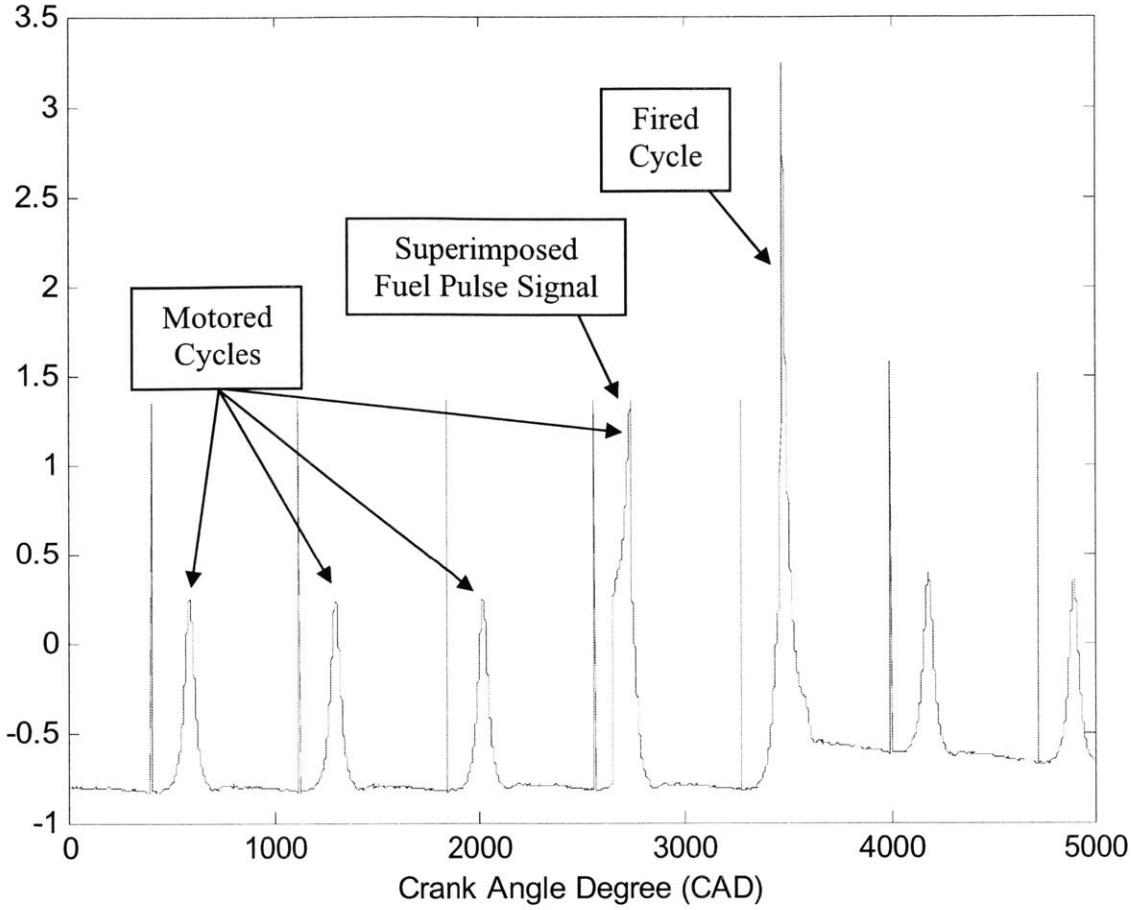

Chapter 2

EXPERIMENTAL APPARATUS

2.1 Modified Spark Ignition Engine

All testing was completed on a production 4-valve per cylinder, 4-cylinder, 2.0L Nissan SR20DE engine, using port fuel injection with a stock injector. See Figure 2.1 and Table 2.1. The engine was previously modified to run as a single-cylinder engine. Since it was driven by a motoring dynamometer, only steady-state, skip-firing operation was to be examined. Cylinder #4 was isolated from the non-firing cylinders by separating the intake and exhaust runners, then venting the intake runners for the non-firing cylinders to the atmosphere. This apparatus allows for more precise control and measurement of the processes in Cylinder #4.

The stock 4-hole fuel injector was located 216 mm upstream from the intake valve seat. Using a known calibration of injected fuel volume vs. pulse width, the injected mass could be calculated based on a measured pulse width and known fuel density. See Figure 2.2 for the injector calibration curve. To vary the injected mass, a variable pulse generator was used with the engine timing signal as a trigger. The driving pressure across the injector was kept constant by referencing the fuel rail pressure to the MAP. To ensure closed valve injection, the start of injection was set to 90 CAD before top dead center (BTDC) during the compression stroke.

To correctly phase the engine events, a digital shaft encoder was connected to the crank pulley. It produced one digital pulse every CAD, as well as an additional signal every revolution to mark the engine position. Spark timing was manually controlled with 1 CAD precision. For all tests, spark timing was fixed at TDC.

2.2 Dynamometer Pulley System

Since the modified engine could not power itself in skip-firing mode with only one firing cylinder, the engine was driven by a Dynamatic 100 hp dynamometer (Figure 2.3) capable of both motoring the engine and absorbing the power from the fired cycles. The dynamometer's stable operating regime was between 900 and 2700 RPM, too fast for cranking speeds. In a previous project, a gear reduction pulley system was added to reduce the engine speed by a ratio

of 3:1. [12] See Figure 2.4. Thus, the dynamometer was capable of speeds slow enough to simulate cranking.

2.3 Temperature Control System

The major modification to the existing engine setup made for this research was to rebuild the engine cooling system with a heater/chiller. See Figure 2.5. A Polyscience 6105 recirculating heater/chiller was used to control the engine coolant temperature (ECT) between -10°C and 80°C. Coolant was constantly circulated through the engine, chiller, and reservoir tank with an external pump to maintain the engine at a constant temperature throughout testing. The engine's factory water pump impellor and thermostat had been previously removed. The engine temperature was verified by reading the coolant temperatures at both engine inlet and outlet, using thermocouples.

In addition, a Neslab RTE-110 bath chiller was used to cool the fuel at the fuel rail during cold testing. This was done using the fuel pump and the pressure regulator return system to pump fuel through the rail and then through a loop of copper tubing immersed in the chiller. Fuel temperature could be matched to ECT down to -10°C, verified using a thermocouple mounted in the fuel rail near the injector.

The intake air temperature was not controlled. The air temperature may be modified somewhat through heat transfer from the port wall, but since most of the fuel lands on the port surfaces, the effect of the air temperature should not be significant.

2.4 In-cylinder Pressure Measurement

Pressure inside the engine cylinder was measured with a Kistler 6051 piezoelectric pressure transducer mounted through the back of the cylinder head. See Figures 2.6 and 2.7. The transducer output signal was amplified using a Kistler charge amplifier and then sent to the data acquisition system. The pressure transducer was calibrated using a dead weight testing system. See Figure 2.8 for the calibration curve.

Two additional signals were superimposed on the pressure trace during testing: the BDC compression pulse, and the fuel injection pulse. The pressure transducer is only capable of measuring the relative change in in-cylinder pressure, rather than absolute pressure. Therefore, a reference is needed to determine the absolute pressure. This reference point is commonly taken

as the MAP at BDC compression; since the intake valve is still open and the piston is instantaneously not moving, at low speeds such as during cranking there is no significant pressure drop across the valve and the cylinder pressure equals the MAP. The fuel injection pulse was superimposed on the pressure trace to reduce the size of the data file, since the fuel pulse could be separated from the pressure trace during post processing. See Figure 1.3 above. Using the injector calibration, injected mass was calculated from this data.

2.5 Fast Flame Ionization Detector

The in-cylinder air-fuel ratio (AFR) was determined using a Cambustion HFR400 Fast Flame Ionization Detector (FFID). The FFID works as follows. A vacuum pump connected to the FFID Main Control Unit (MCU) draws in a continuous sample from the combustion chamber, through a sampling tube inserted through a special Sampling Spark Plug (SSP). See Figures 2.6 and 2.7. The tube is heated by an external Line Heater Controller (LHC) to 180°C, to prevent any fuel from condensing in the sampling line. Thus, the sample reaching the Hydrocarbon Sampling Module (HSM) would be the same as the in-cylinder sample. When the sample reaches the HSM, it is burned in a hydrogen-air flame, resulting in the production of ions. For HC fuels, the number of ions is nearly proportional to the number of carbon atoms in the fuel. Therefore, by using an ion collector to produce a signal in response to ion formation, the output is generated in proportion to the concentration of HC in the sample. This output is amplified in the MCU and subsequently output to the data acquisition system as a voltage.

Since the output depends on the mass flow rate entering the sample chamber, the Cambustion FFID is designed to provide a constant mass flow rate irrespective of conditions inside the cylinder. The MCU pressure controller regulates the pressure difference across the sample tube and the gauge pressure in the constant pressure (CP) chamber. In order to produce meaningful data for the entire intake process, the CP chamber must be operated at very low absolute pressure. Without this system, there would be no flow into the HSM when cylinder pressure is sub-atmospheric during the intake stroke, but rather backflow into the cylinder. To achieve a higher vacuum level, an extension chamber was added to the main CP chamber in the HSM. Typical values were 100 mmHg vacuum for the pressure drop across the sampling tube and 400 mmHg for the CP vacuum.

The response of the FFID drifts slowly over time, thus calibration was necessary before and after each test. To calibrate the in-cylinder sample, the sampling probe was removed from the engine and placed in a bench testing rig. Using a volume flow rate controller, known mixtures of pure propane (C_3H_8) and air were flowed past the sampling probe, and the FFID calibrated to give a linear response. Typically, the FFID was calibrated using 0%, 2%, 4%, and 8% propane-air mixtures.

2.6 Data Acquisition System

All data was acquired using a Dell Pentium III computer with a National Instruments PCI-6025E multi-function I/O board, National Instruments BNC-2090 BNC connector board, and Labview 5.1 data acquisition software. The data acquisition software was triggered by the crank angle signal from the shaft encoder, such that data was recorded once every CAD. Only two channels of data were recorded: the pressure trace with superimposed BDC and fuel pulses as described above, and the FFID output.

2.7 Engine Operating Conditions

The first cycle of cranking for a given cylinder is unique because there are no residual burned gases from the previous fired cycle. Furthermore, the first cycle is also unique because of the state of liquid fuel in the port and cylinder. For a normal shutdown, there may be some residual fuel in the port and/or cylinder due to injected fuel that was neither burned nor exhausted when the engine was stopped. However, this condition is not controlled and therefore varies from one shutdown to the next. For a repeatable starting condition, it is assumed that there is no residual liquid fuel in either the port or cylinder. Thus, this condition is different from subsequent cycles, when the fraction of liquid fuel that did not enter the combustible mixture remains in the port and/or cylinder.

To eliminate the residual gases from the first cycle and to purge the engine of residual liquid fuel, the engine was operated in a skip firing mode, where fuel is injected only once and then many cycles are skipped, until the FFID shows a negligible level of HC in the cylinder. Depending on the ECT and injected fuel mass, between 30 and 300 cycles were typically skipped.

To simulate cranking, the engine was motored at a constant 300 RPM. The MAP was then adjusted to 0.92 bar with a throttle valve. This value is based on research by Cowart and Castaing [11] correlating MAP to cranking speed on a 4-cylinder engine. With the speed and MAP stabilized, FFID data was checked until the in-cylinder HC was nearly zero (e.g. less than 0.05%). Once the clean engine state was determined, fuel was injected once, and then not injected again until the clean engine state was regained. This strategy yielded an engine condition very close to real cranking that could be repeated over many cycles without having to fully warm up and shut down the engine.

ECT was maintained at the test temperature by the recirculating chiller system. Test temperatures were -6°C, 10°C, 20°C, 40°C, and 80°C. For the two coldest temperatures, the fuel was also chilled, since cold ambient conditions would cool all components and substances to said temperature. For the warm and hot tests, the fuel would not remain as hot as the coolant, and thus was not heated separately.

Table 2.1 – Nissan Engine Specifications

Configuration	4-valve per cylinder, DOHC Aluminum block/head
Bore x Stroke (mm)	86 x 86
Connecting Rod Length (mm)	136.3
Cylinder Displacement (cm^3)	500
Clearance Volume (cm^3)	58.77
Compression Ratio	9.5:1
Intake Valves (34 mm diameter, 10.2 mm maximum lift)	Open 13 CAD BTDC Close 235 CAD ATDC
Exhaust Valves (30 mm diameter, 9.44 mm maximum lift)	Open 483 CAD ATDC Close 723 CAD ATDC
Valve Overlap	16 CAD

Figure 2.1 – Modified Nissan Engine

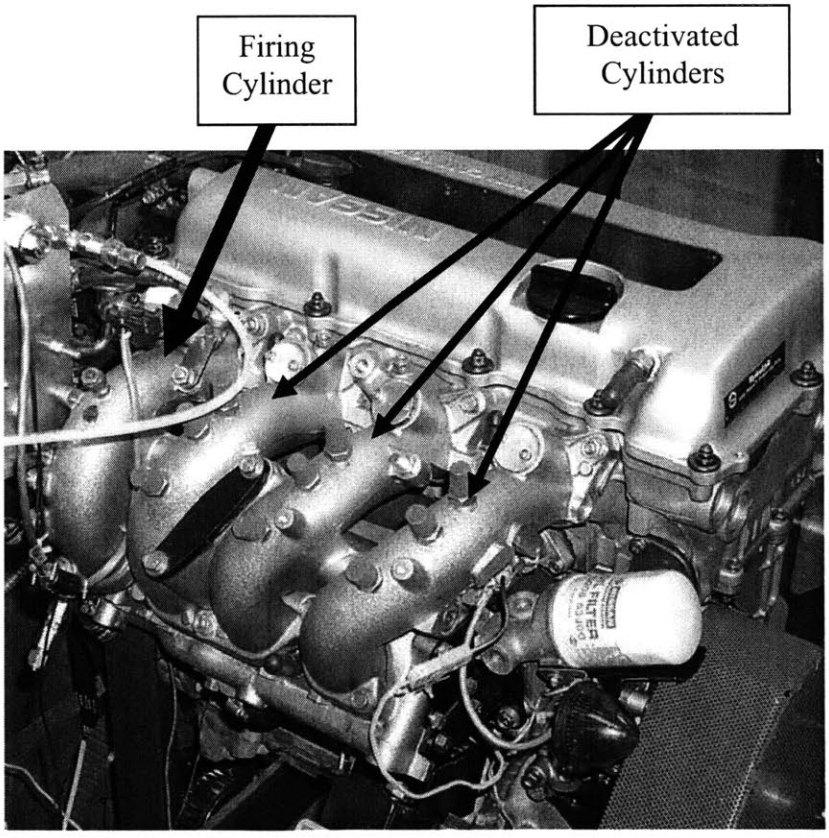

Figure 2.2 – Fuel Injector Calibration Curve

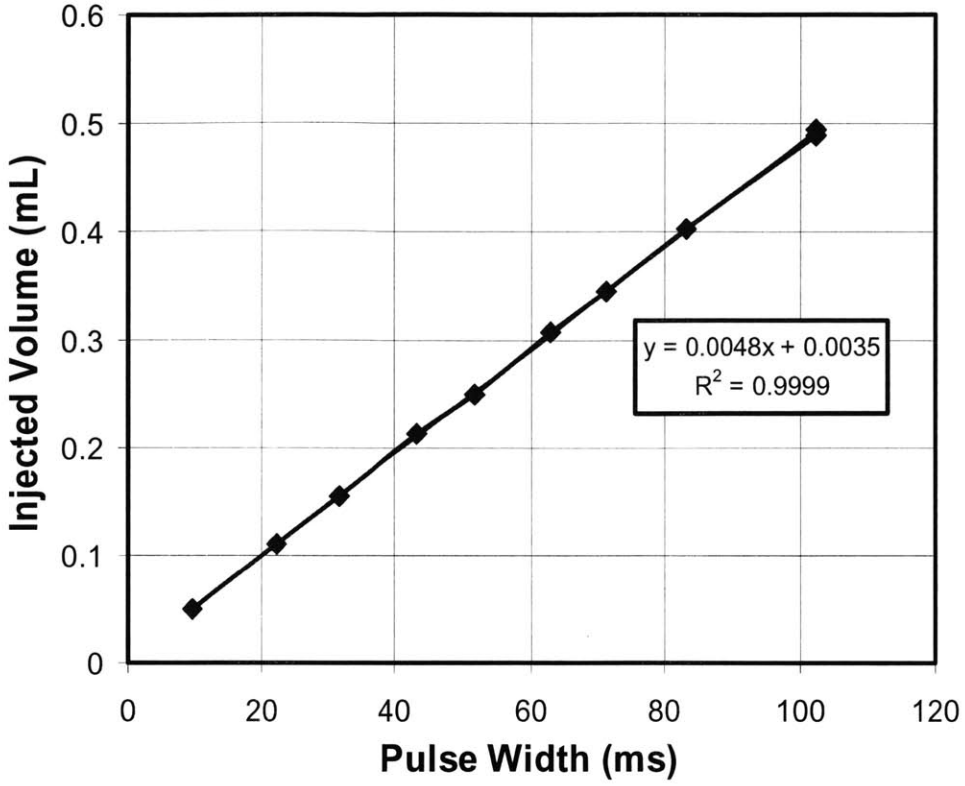

Figure 2.3 – Dynamometer

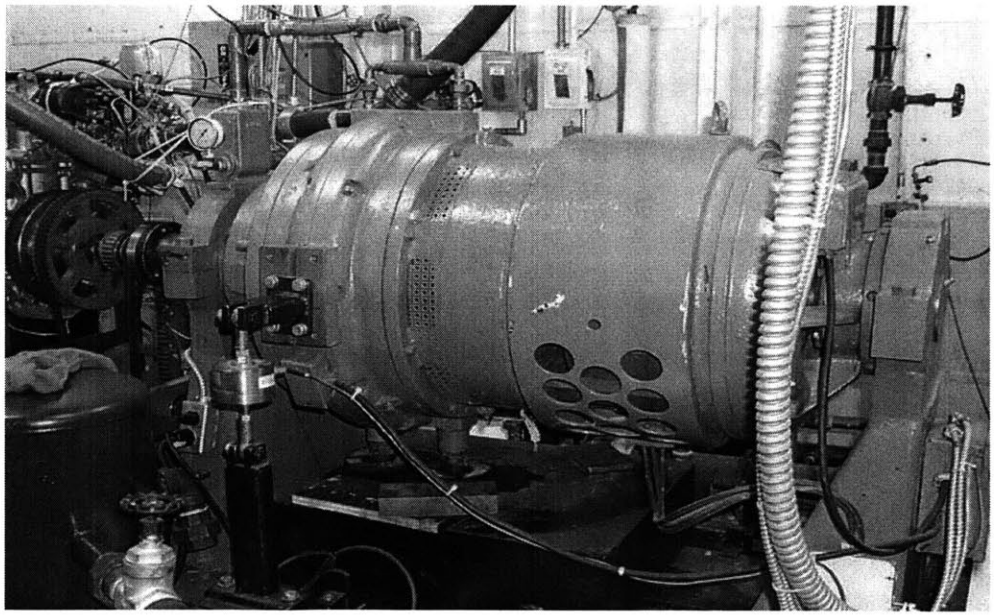

Figure 2.4 – Dynamometer Pulley System

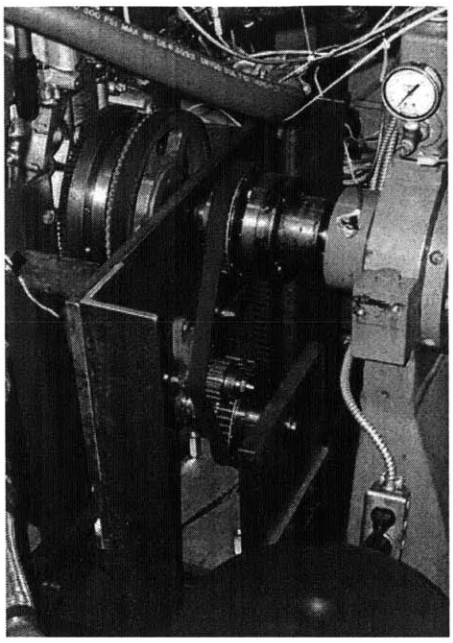

Figure 2.5 – Heater/Chiller System

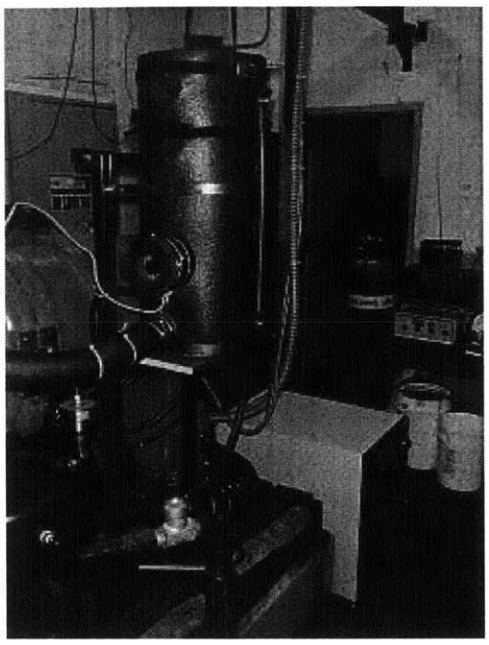

Figure 2.6 – Instrumentation and Key Features of Combustion Chamber (Front View)

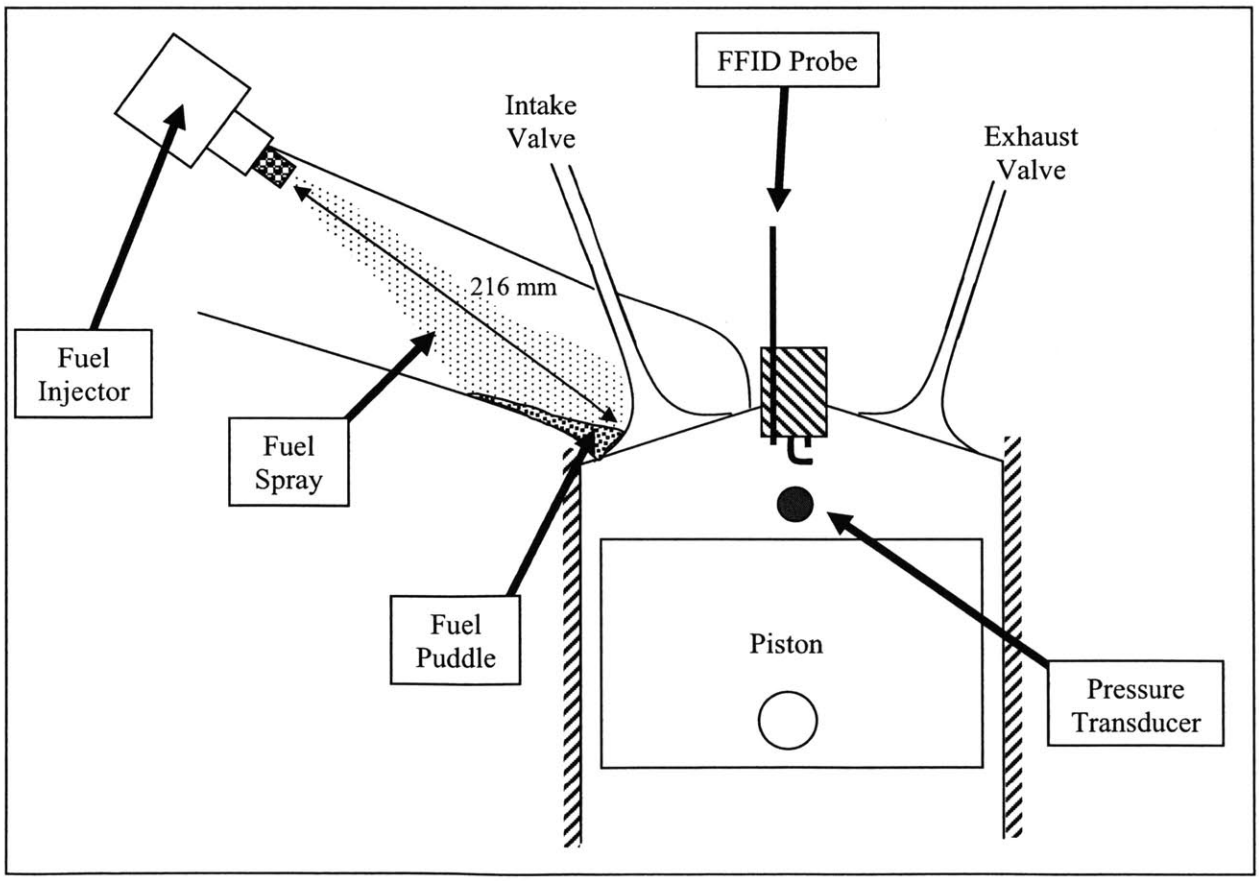

Figure 2.7 – Instrumentation and Key Features of Combustion Chamber (Top View)

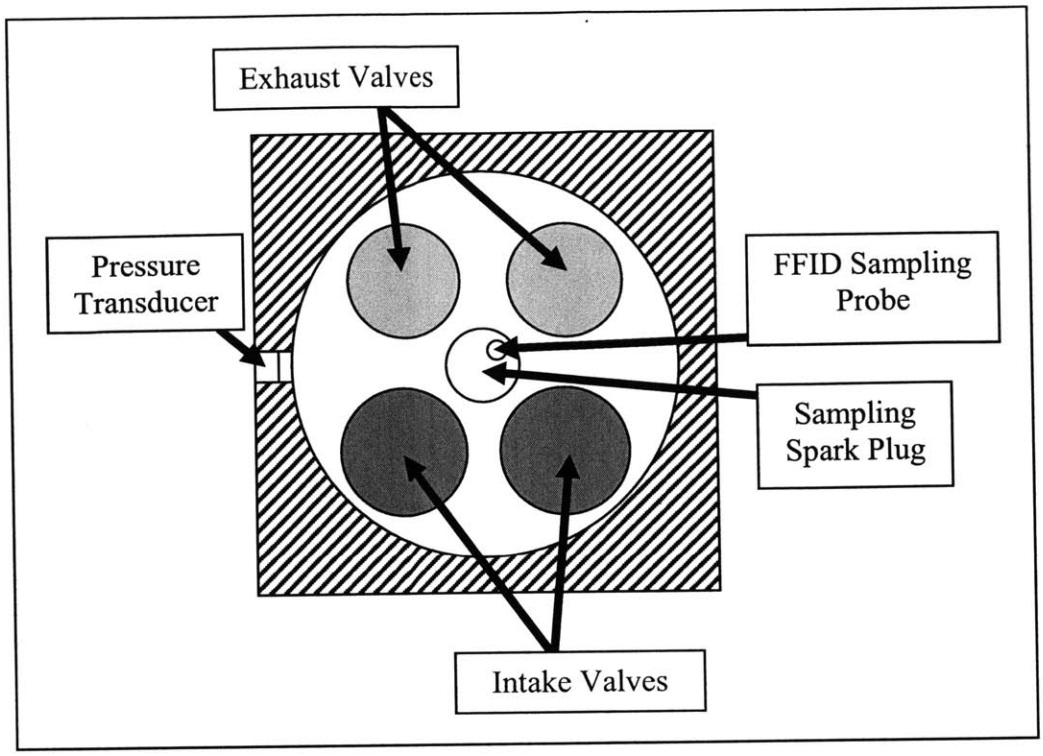

Figure 2.8 - Pressure Transducer Calibration Curve

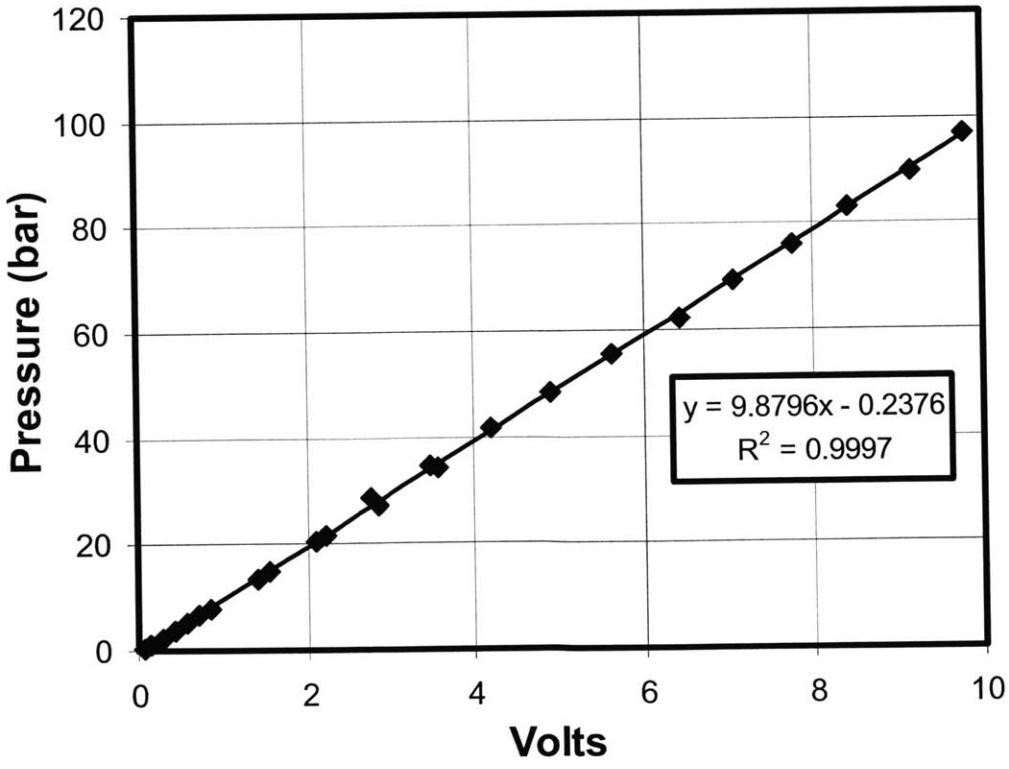

Chapter 3

FUEL DELIVERY TEST RESULTS

3.1 Overview of Fuel Delivery

Fuel delivery is the process by which liquid fuel is injected into the intake port and then mixed with fresh air to form a combustible mixture. Combustion and emissions in SI engines depend strongly on fuel delivery, since a stoichiometric mixture is needed for clean, robust combustion. A substantial amount of energy is needed to vaporize liquid fuel. This energy must come from one of three sources: the intake port wall/intake valve, the intake air, and/or the fuel itself. Subsequently, factors affecting fuel delivery include the state of the intake port, fuel injection, and fuel properties.

3.1.1 Intake Port State

The state of the intake port has significant impact on fuel delivery. In a fully-warmed engine, the intake valve is heated to elevated temperatures by the combustion gases. The fuel injector is aimed at the back of the closed intake valve, and the injected fuel quickly and effectively vaporizes upon hitting the hot valve. Thus, the energy for vaporization comes primarily from thermal energy stored in the mass of the valve and port wall. For the first cycle, however, the valve and port are generally at ambient temperature, except in the case of a hot restart. For cold starts, the energy to vaporize fuel must come from another source.

3.1.2 Fuel Injection and Atomization

Preparing the mixture of air and fuel vapor requires evaporation of liquid fuel by one of three processes in a PFI engine: direct atomization of airborne fuel droplets from the injector, strip atomization of the liquid wall film by back flow from the cylinder gases when the intake valve opens, and strip atomization of the wall film by forward flow during intake.

To achieve better mass transfer, the fuel injector atomizes the liquid fuel into fine droplets to provide more surface area for vaporization and to cover a broader area of the intake port with the fuel film. However, PFI engines use relatively low-pressure injectors, typically 3 to 4 bar compared to 1000 bar in Diesel engines. This results in droplets on the order of 100 μm.

[12] These relatively large droplets primarily land on the port walls and form a liquid film, as shown in Figure 2.6 above.

For the first cycle of cranking, back flow from the cylinder is not an effective means of vaporization since the intake manifold pressure has not yet been drawn down, thus there is little driving force across the intake valve to produce an effective back flow; the brief displacement flow from the cylinder is not a significant contributor to fuel delivery. Moreover, since there is no previous fired cycle, cold gases are displaced into the port.

Forward strip atomization is the primary process for fuel delivery during the first cycle. As the fuel film sits on the port wall, some of the liquid fuel will have enough energy to vaporize and will be carried into the cylinder by the intake air flow. During the intake stroke, convective mass transfer occurs between the liquid fuel film and the fresh intake air. However, due to near-atmospheric MAP, vaporization is more difficult than at lower MAP such as during idle.

For given flow conditions, however, the temperature of the air itself does not significantly affect fuel delivery. A study by Heywood and Meyer found that changing the charge air temperature had negligible affect on fuel evaporation. [13] Thus, even with more energy present in the air, more of that energy did not transfer to the fuel. This suggests that heat transfer from the air is not a significant contributor to fuel delivery.

3.1.3 Fuel Properties

Commercial gasolines typically contain more than 100 chemical species, each with different boiling points and evaporative properties. The more volatile components will vaporize at a lower temperature than the less volatile components; this progressive evaporation is reflected in the industry standard test of gasoline volatility, the ASTM D86-04 distillation test. The test measures the percent by volume of fuel that evaporates at a given temperature, at atmospheric pressure. T10, T50, and T90 from the ASTM D86-04 test are used to calculate DI, as described above.

Another industry-standard fuel property is the Reid Vapor Pressure (RVP), as measured by ASTM D323. RVP is in indication of the fuel's volatility based on the pressure generated by the vapor-air mixture at a given temperature (37.8°C); a more volatile fuel will yield more vapor, and thus a higher RVP.

For the first cycle of cranking, there is limited energy available to vaporize liquid fuel. Thus, the evaporative properties of the fuel might be a limiting mechanism for fuel delivery – for given conditions external to the fuel, a more volatile fuel will result in better fuel delivery. The effect of fuel properties on fuel delivery were therefore tested experimentally.

Four different fuels were tested at each of the five temperatures. Three of the fuels, hereafter referred to as Base Fuel, Fuel #1, and Fuel #2, were custom blended by ExxonMobil to compare the effect of specific portions of the distillation curve. Thus, the most critical region of the distillation curve might be identified, in order to better characterize fuel delivery based on known fuel properties. A fourth fuel, hereafter referred to as High DI Fuel, was chosen for low overall volatility. The distillation curves and other fuel properties for all four fuels are shown in Figure 3.1. The left side of the distillation curve shown in Figure 3.1 represents the most volatile components of the fuel. Moving to the right, the remaining components are less and less volatile, and thus require higher temperatures in order to vaporize.

At a given distillation percentage, a higher temperature indicates a less volatile fuel, and a lower temperature indicates a more volatile fuel. Conversely, for a given temperature, a greater percentage evaporated indicates a more volatile fuel, and vice versa. Note that for the fuels tested, the relative volatilities are different at different points on the distillation curve. With the exception of the High DI fuel, no fuel is clearly more or less volatile than the others.

3.2 Test Results

3.2.1 Typical In-Cylinder FFID Signal

To determine the effect of fuel properties on first cycle fuel delivery, the in-cylinder HC level was measured using the FFID with the SSP. To ensure closed valve injection, the start of fuel injection was set to 90 CAD after bottom dead center (ABDC) of the compression stroke. Spark timing was set at TDC to allow as much time as possible for the in-cylinder mixture and thus the FFID reading to stabilize.

Figure 3.2 shows a typical FFID trace, along with the cylinder pressure, injection pulse, and valve events, for skip firing. The initial HC level is zero, since the engine has been purged by skipping injection for many cycles. The fuel pulse shown in Figure 3.2 represents a 100 ms pulse at 300 RPM cranking speed; the first fuel from that pulse resides in the intake port for 437 CAD before intake valve opening (IVO). After IVO, there is some transport delay until the first

sample of air-fuel mixture reaches the FFID. The increase in the in-cylinder FFID signal corresponds to rapidly rising HC concentration in the cylinder: the air-fuel mixture entering the cylinder is initially very rich, due to a pocket of vaporized fuel and possibly some liquid droplets which reside near the intake valve and thus enter the cylinder immediately after IVO. This initial rich peak represents the individual fuel molecules that are most likely to vaporize, either during injection or during the residence period in the intake port. As this fuel evaporates, it carries with it energy from the remaining puddle of liquid fuel. Thus, the air-fuel mixture later in the intake stroke becomes increasingly lean, as the remaining liquid fuel has less energy for vaporization.

After intake valve closing (IVC), the inhomogeneous air-fuel mixture is trapped in the cylinder, and it mixes due to turbulence in the combustion chamber. This is also seen in Figure 3.2, as the FFID signal stabilizes as the piston approaches TDC. The stabilized value near TDC is then used to calculate the in-cylinder AFR. Immediately after the spark, the FFID signal rapidly drops to zero as the fuel is burned – since the SSP is used, the FFID is measuring the HC concentration at the spark plug itself, and hence this region burns first. As the HC drops to zero, the pressure increases rapidly due to combustion. After combustion is complete, the HC concentration rises slightly due to out-gassing from the crevice volumes, e.g. the spark plug, piston rings, and the SSP itself.

3.2.2 Calculation of In-Cylinder Equivalence Ratio and Fuel Delivery Fraction

The FFID was calibrated against known mixtures of propane (C_3H_8) and air, such that the FFID output is the HC mole fraction of CH_n. Gasoline is a mixture of many different molecules, but it can be represented overall by $(CH_n)_q$, where n is the ratio of hydrogen to carbon atoms, and q is used to match the average molecular weight of the fuel. For all fuels used in the tests, n = 2.1, and q = 7.8, based on an average molecular weight of 110. Thus, the fuel was assumed to be $(CH_{2.1})_{7.8}$.

The in-cylinder AFR, and thus equivalence ratio, can be determined using the following expressions, where Y, n, m, and M represent mole fraction, number of moles, mass, and molecular weight, respectively. For these fuels, the stoichiometric AFR (AFR_S) is 14.922.

$$Y_{CH_n} = \frac{qn_f}{n_f + n_a} = \frac{q}{1 + {n_a}/{n_f}} = \frac{q}{1 + \left({m_a}/{m_f}\right)\left({M_f}/{M_a}\right)} = \frac{q}{1 + (AFR)\left({qM_{CH_n}}/{M_a}\right)}$$

$$\Phi = \frac{AFR_S}{AFR} = \frac{AFR_S}{\left(\frac{1}{Y_{CH_n}} - \frac{1}{q}\right)\left(\frac{M_a}{M_{CH_n}}\right)}$$

Thus, with the known calibration of the FFID, the output voltage is converted into mole fraction of CH_n, which is then input into the above expression to calculate Φ. For rich mixtures, $\Phi > 1$, and for lean mixtures, $\Phi < 1$.

The first cycle Φ describes the strength of the in-cylinder AFR, but it gives no indication of the effectiveness of the fuel delivery process. However, the fuel delivery fraction, defined as the fraction of injected fuel mass that enters the air-fuel mixture, can be calculated. Neglecting the small contribution of the fuel vapor's partial pressure (typically less than 0.04 bar), and since there is no residual gas for the first cycle, the mass of air trapped in the cylinder can be estimated using the ideal gas law, knowing the intake pressure and the trapped volume at IVC.

$$m_a = \frac{P_{in} V_{IVC}}{R_a T_a}$$

The trapped fuel mass inside the cylinder can then be estimated using the following expression. This assumes that the air-fuel mixture inside the cylinder is homogeneous. While not strictly true, Figure 3.2 shows how the FFID signal stabilizes near TDC, indicating near-homogeneity.

$$m_f = \frac{(m_a)(\Phi)}{AFR_S}$$

Using this calculated value and the measured value of injected fuel mass, the fuel delivery fraction can be calculated.

3.2.3 Effect of ECT

Before examining the effect of fuel properties, the effect of ECT on fuel delivery is examined. Figure 3.3 shows Φ vs. injected mass for the Base Fuel only, as these results are typical of ECT dependence. As more fuel mass is injected, Φ increases due to the higher amount of fuel in the port, relative to the mass of air. At colder temperatures, however, substantially

more fuel must be injected to achieve a combustible mixture, defined here as $\Phi \geq 0.8$ for purpose of comparison. Figure 3.4 shows the fuel delivery fraction as a function of injected mass and temperature. At high temperatures, when the port walls and back of the intake valve can provide thermal energy to vaporize the fuel, the delivery fraction is high, up to nearly 90%. However, delivery fraction also drops as injected mass increases. This is due to the fact that there is limited energy available for vaporization, and a greater mass of injected fuel would require more energy to vaporize the same fraction. These results confirm data previously reported in [12].

3.2.4 Effect of Fuel Properties

Figure 3.5 shows Φ vs. injected mass for all four fuels, for each test temperature. As expected from the distillation curves, the High DI fuel yields lower Φ, i.e. worse fuel delivery, under all conditions. The distillation curves show that the High DI fuel requires more energy to vaporize, and given the limited energy available for fuel delivery, the other fuels yield more vapor and thus a richer mixture.

Figure 3.6 shows the fuel delivery fraction for all four fuels, for each test temperature. The same overall trends described above for the Base Fuel still apply, but comparing the Base Fuel to Fuel #1 and Fuel #2, there are no consistent trends across all conditions. The relative fuel delivery behavior depends on both temperature and injected mass.

A more meaningful representation of the data is to consider the injected mass required to achieve a combustible mixture, assumed for this purpose to be $\Phi \geq 0.8$. Figure 3.7 shows the required injected mass as a function of temperature for each fuel. For the tests at -6°C, nearly an order of magnitude greater injected mass was required to achieve a combustible mixture compared to the tests at 80°C. Figure 3.7 also shows how, at cold temperatures, Fuel #1 yields better fuel delivery than the Base Fuel, and both are better than Fuel #2. As temperature increases, however, Fuel #1 and the Base Fuel are approximately equivalent, and Fuel #2 yields better fuel delivery.

3.2.5 Effect of Fuel Temperature

Since the fuel itself is one of the primary sources of energy for vaporization, the effect of fuel temperature was evaluated for the two coldest test temperatures, -6°C and 10°C. Tests were conducted at both ECTs with no fuel chilling, such that heating due to the pumping loop resulted

in a fuel temperature of 35°C. Those tests were repeated with the fuel chilled to match the ECT. Figure 3.8 shows the effect of fuel temperature on Φ for the first cycle for -6°C ECT, and Figure 3.9 shows the effect of fuel temperature for 10°C ECT.

At -6°C ECT, reducing the fuel temperature from 35°C to -6°C typically resulted in a 30% reduction in Φ. At 10°C ECT, reducing the fuel temperature from 35°C to 10°C typically resulted in a 10-20% reduction in Φ. These results confirm that the internal energy of the fuel itself is contributing to fuel delivery.

Figure 3.1 – Distillation Curves and Fuel Properties for Test Fuels

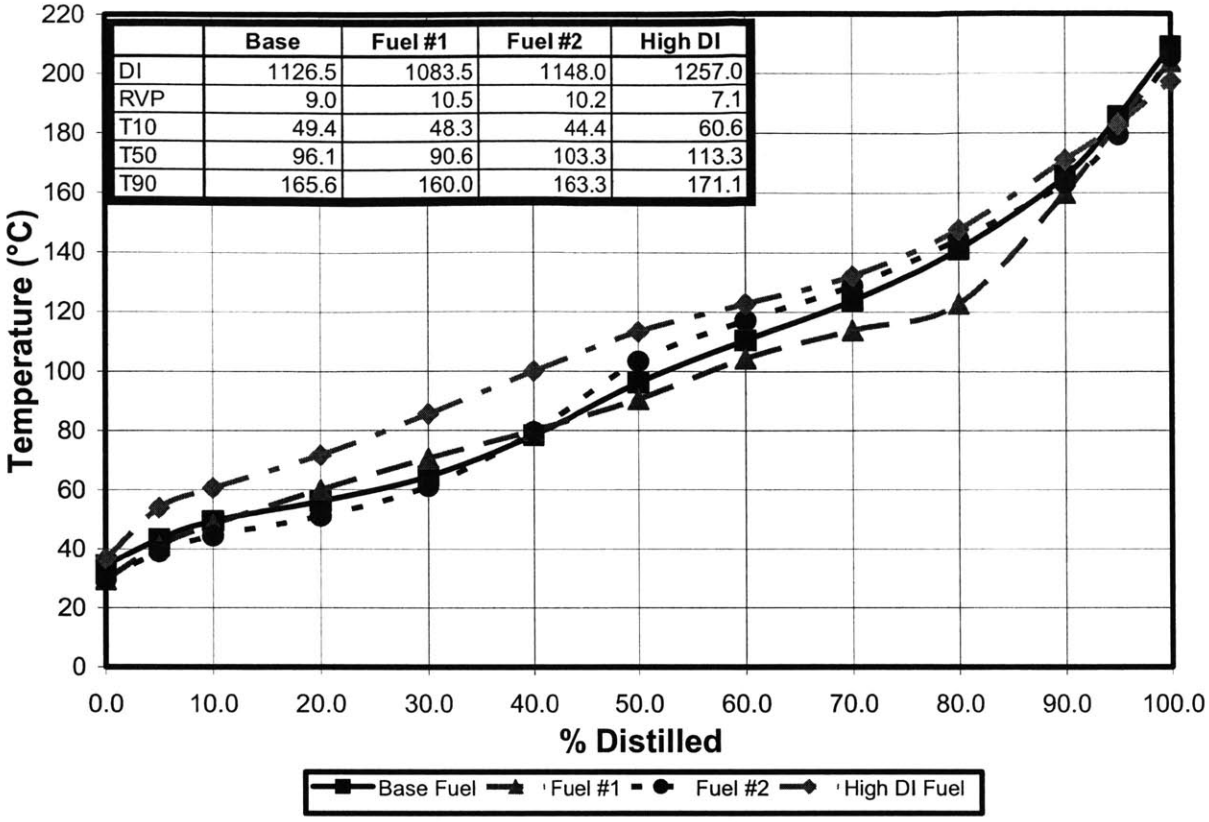

Figure 3.2 – Typical FFID and Pressure Traces, with Valve and Injection Events

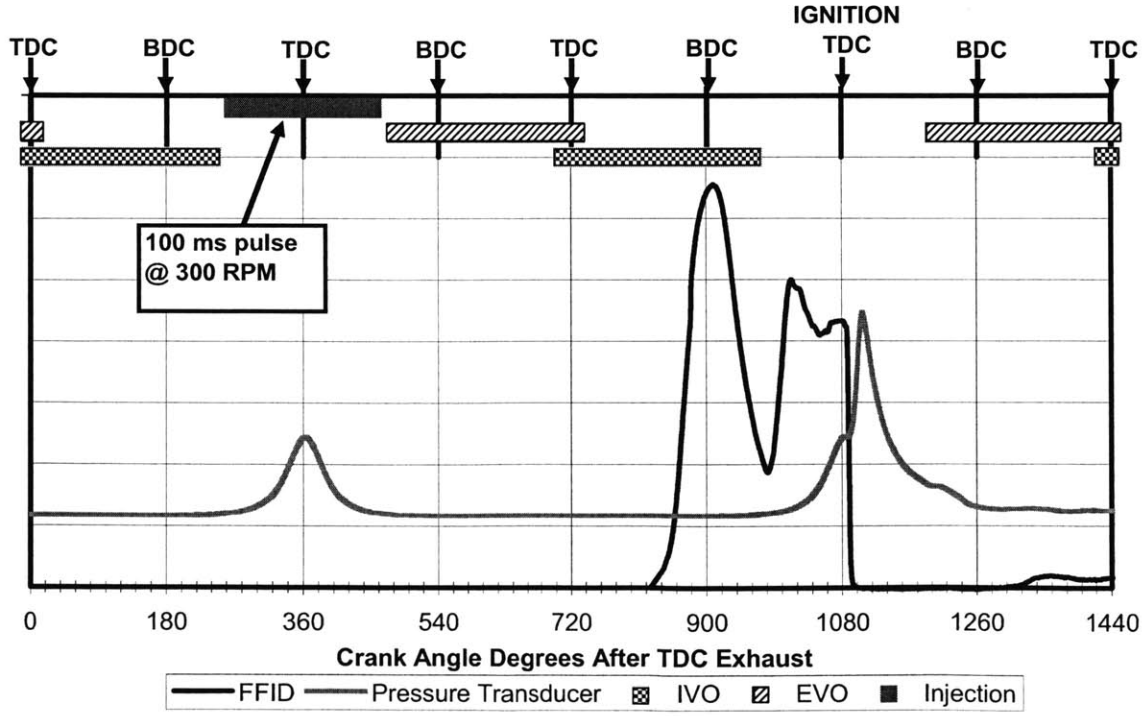

Figure 3.3 – Effect of ECT on Φ vs. Injected Mass for Base Fuel

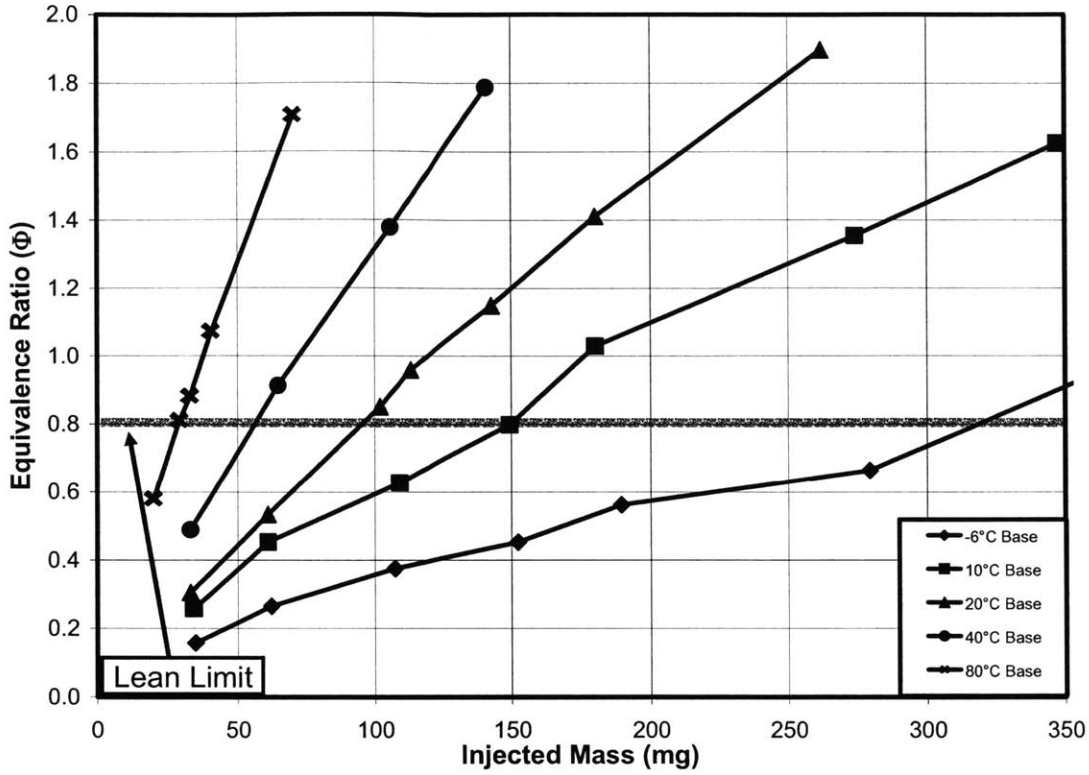

Figure 3.4 – Effect of ECT on Delivery Fraction vs. Injected Mass for Base Fuel

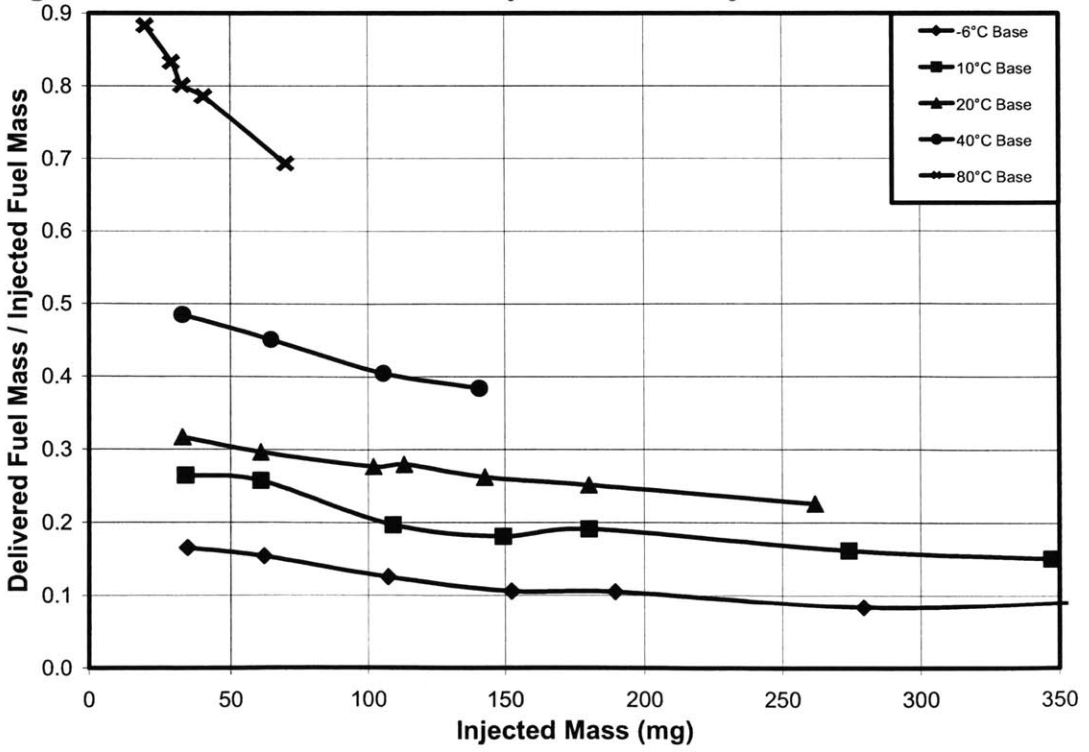

Figure 3.5 - Effect of Fuel Properties on Φ vs. Injected Mass

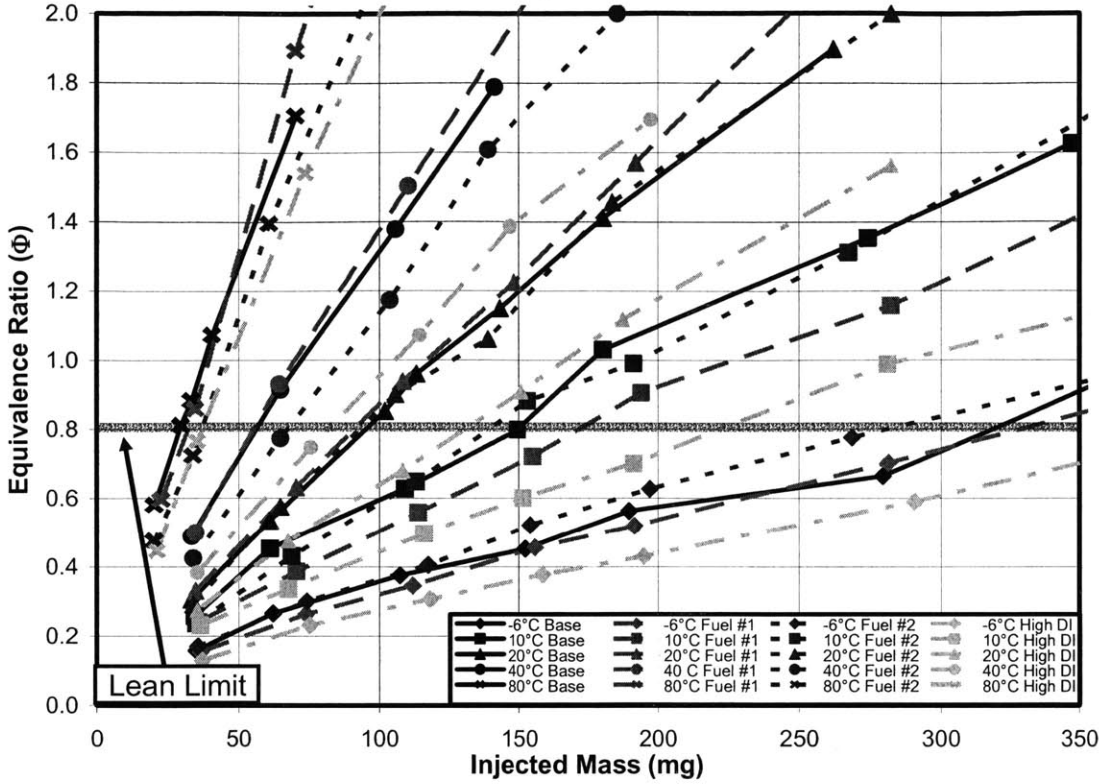

Figure 3.6 – Effect of Fuel Properties on Delivery Fraction vs. Injected Mass

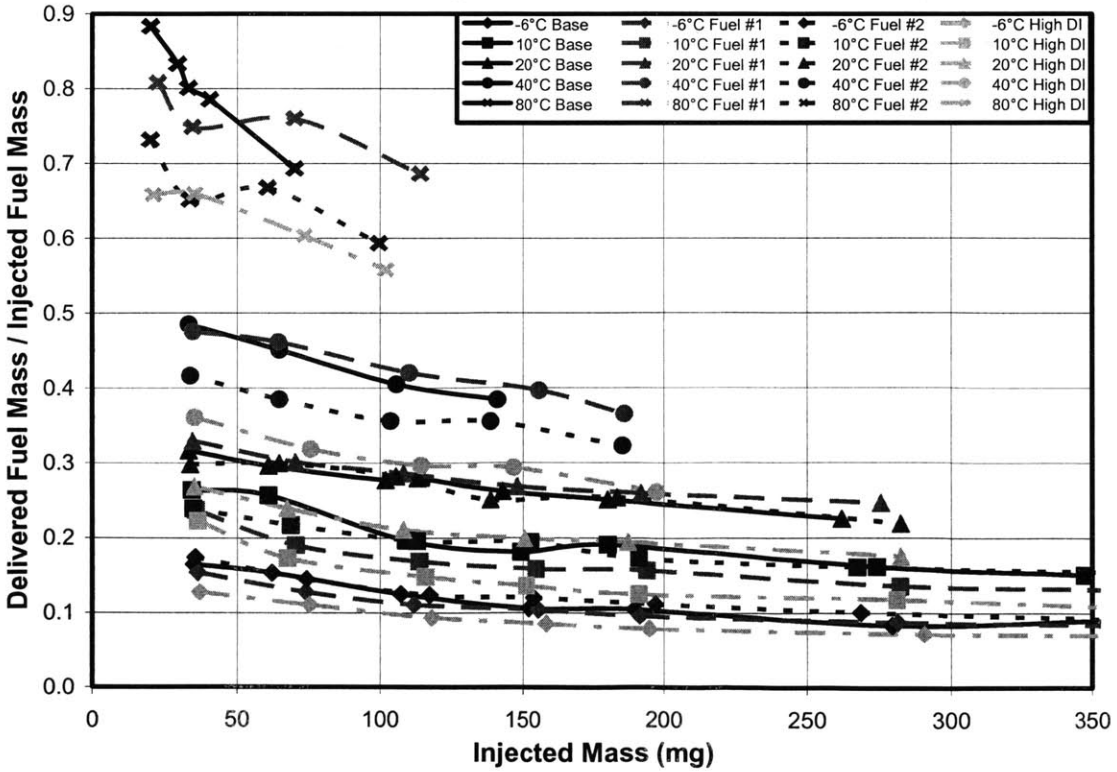

Figure 3.7 – Required Injected Mass for Φ = 0.8 vs. Temperature

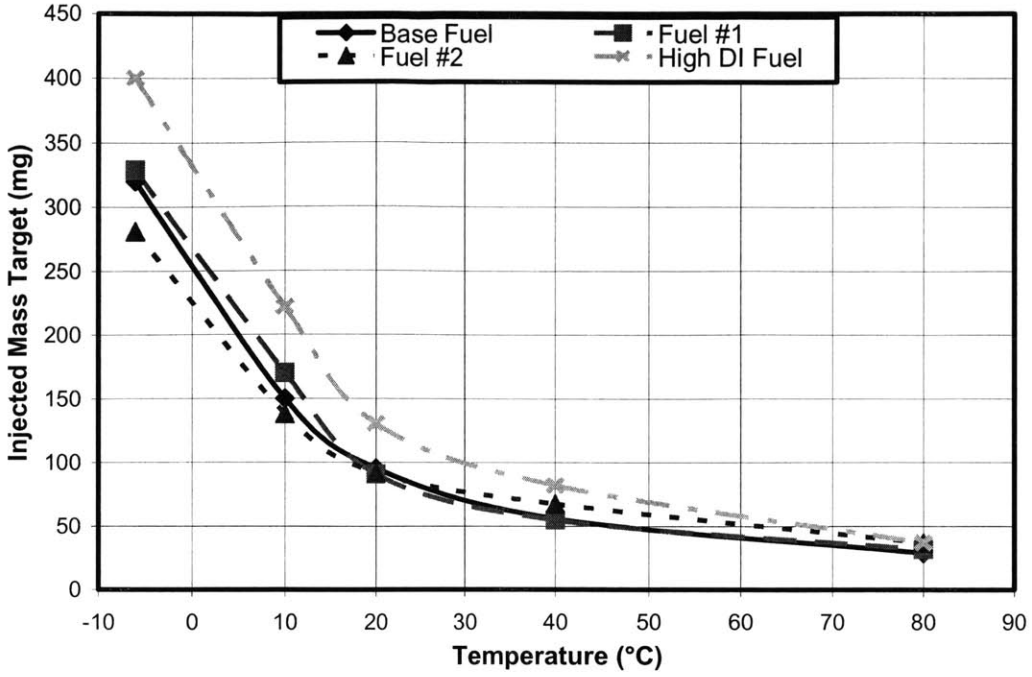

Figure 3.8 – Effect of Fuel Temperature on Φ vs. Injected Mass for –6°C ECT

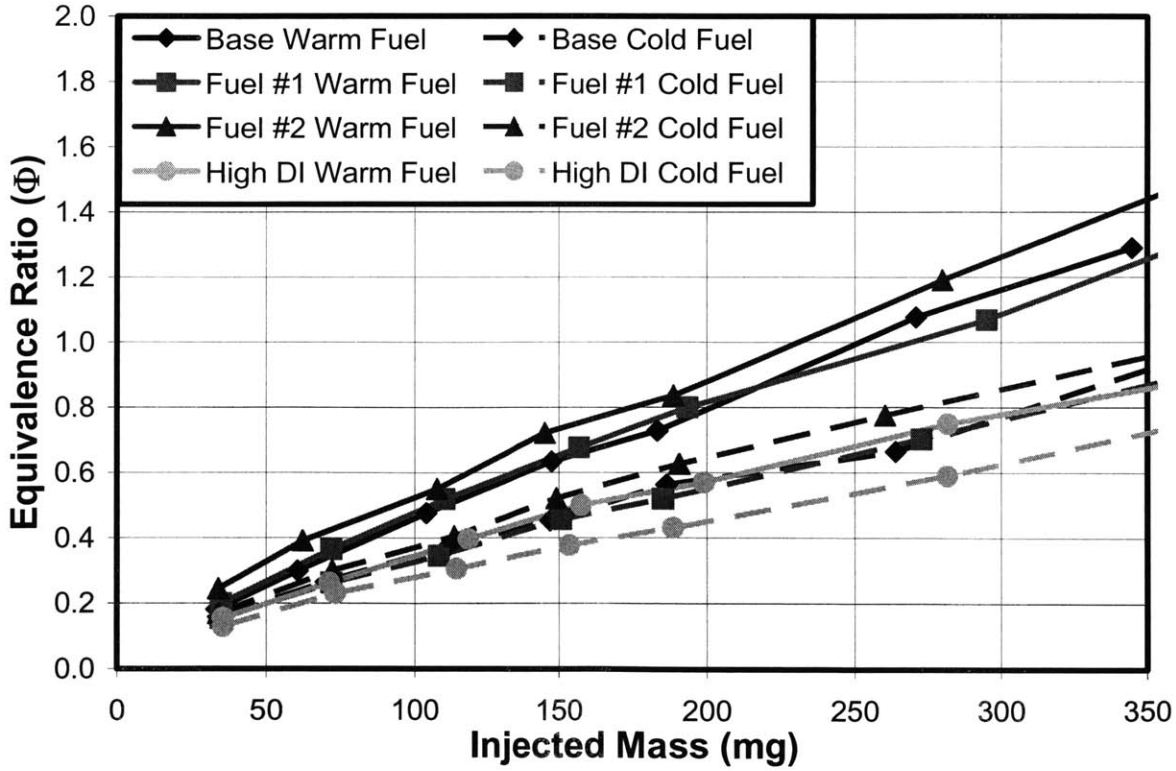

Figure 3.9 – Effect of Fuel Temperature on Φ vs. Injected Mass for 10°C ECT

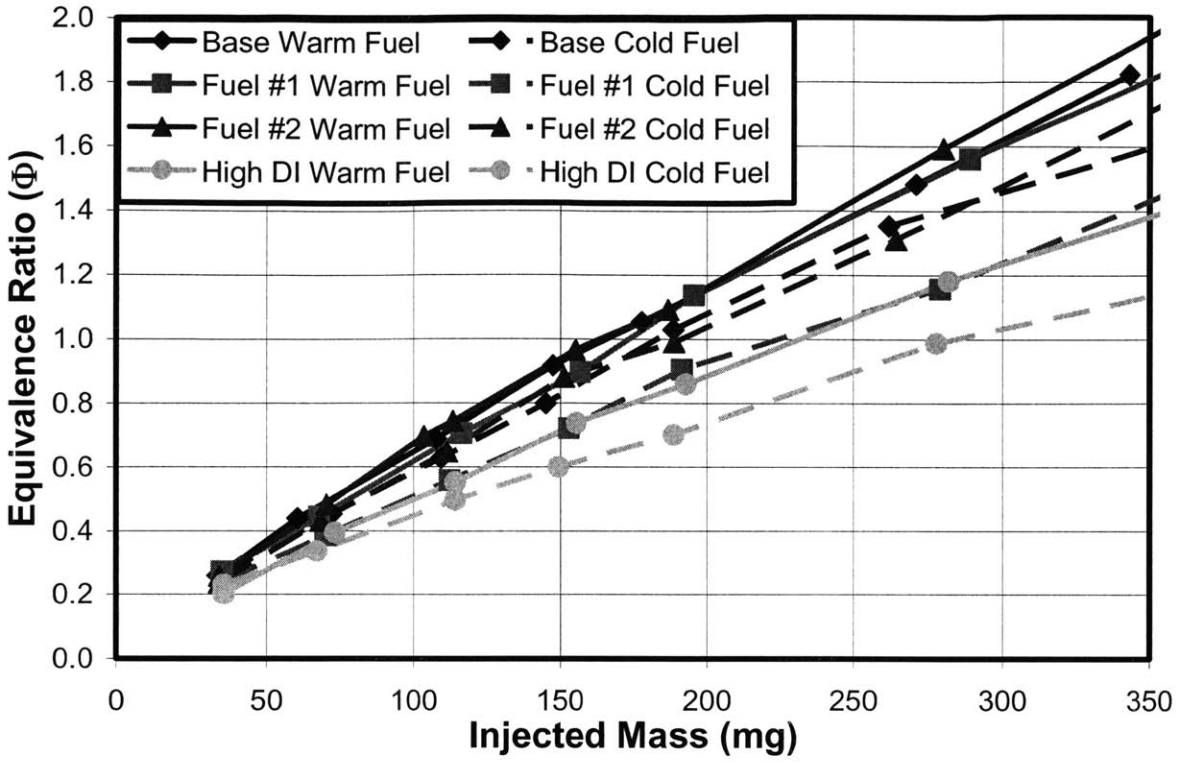

Chapter 4

DATA ANALYSIS

4.1 Range of Mixture Quality

Figure 3.5 showed the broad range of first cycle, in-cylinder Φ that could be achieved for a given injected mass, depending on the fuel. In a real vehicle, the injected mass for the first cycle is prescribed primarily based on ambient temperature, as in-vehicle fuel volatility measurements are not yet practical. [14] Thus, a misfire might result if the first cycle injected mass is calibrated based on a high volatility fuel, and a low volatility fuel is encountered in use. Conversely, if the first cycle injected mass is calibrated based on the worst-case, low volatility fuel, the engine will be over-fueled for any other fuel and HC emissions will be higher than necessary.

To evaluate the range of Φ which might be encountered in a vehicle, the required injected mass to achieve $\Phi = 0.8$ was evaluated at each test temperature, for both the most volatile fuel tested and the least volatile fuel tested. The High DI fuel is the least volatile fuel for all temperatures tested, but the most volatile fuel depends on temperature. Then, the first cycle Φ for each of the other fuels was calculated at these injected mass values, resulting in a range of possible Φ for each test temperature, depending on the fuel used for engine calibration. This process is shown in Figure 4.1, for the case of 20°C. For the most volatile fuel at this temperature, Fuel #1, 92 mg of fuel must be injected in order to reach $\Phi = 0.8$. If this same injected mass were used with the High DI fuel, the engine would misfire due to a lean mixture at $\Phi = 0.6$. For the High DI fuel, 130 mg must be injected to achieve a combustible mixture. If this injected mass were used with Fuel #1, the in-cylinder mixture would be rich, with $\Phi = 1.1$. While this is not rich enough to misfire, it is more fuel than the engine needs, and thus would yield higher HC emissions than necessary.

The summary of this evaluation of the range of mixture quality is shown in Figure 4.2. Depending on the temperature and which fuel is used for calibration, a broad range of Φ is possible, from as lean as 0.56 to as rich as 1.18. These results demonstrate the dramatic impact of fuel properties across the full range of temperatures encountered in the real world, from sub-

freezing cold starts to hot restarts. To fully optimize fuel delivery for the first cycle and thereby minimize HC emissions, engine calibrations must be based on both temperature and fuel properties.

4.2 Correlation of First Cycle Φ Values with DI and with RVP

In current engine development practice, DI and RVP are the most commonly used metrics of fuel volatility, since they are well known for commercially available development fuels. If first cycle fuel delivery could be correlated to either or both of these fuel properties, such a relation could be readily incorporated into the engine management strategy.

To assess this, the injected mass required to achieve $\Phi = 0.8$ was regressed against both DI and RVP. Figure 4.3 shows the required injected mass vs. DI. The R^2 values are significant for the tests at 20°C and 40°C, but for the other temperatures there is no clear relation between DI and fuel delivery. Thus, while using DI to calibrate first cycle fuel injection might yield valid results for a 20°C cold start or a warm restart, the same calibration used for cold temperatures could yield erroneous results and thus high HC emissions. For RVP, the overall correlation is even weaker, with a significant R^2 value only for the data at 20°C.

4.3 Correlation of First Cycle Φ Values with Distillation Points

Although DI is the most commonly used representation of fuel volatility, it is no more readily available than the rest of the ASTM distillation curve. DI is a function of the 10%, 50%, and 90% distillation temperatures, known as T10, T50, and T90. However, to obtain these values, the entire ASTM D86 test procedure must be carried out. Thus, any point along the distillation curve would be a readily available fuel property to use in engine development.

The injected fuel mass required for $\Phi = 0.8$ was regressed against each point on the ASTM distillation curve, including the initial boiling point and end point. The results are shown in Figures 4.5 – 4.17. Several key features of these regressions are worth noting.

For each test temperature, the R^2 values become much less significant above about T60. This suggests that the less volatile fuel components, i.e. those that are least likely to vaporize, have little effect on first cycle fuel delivery. With limited energy available to vaporize fuel, the heavy ends of the distillation curve are likely to remain as liquid fuel. Also worth noting is that there was no clear correlation for the data at 80°C. This is perhaps due to the fact that there is

very little difference in the injected mass required for the least volatile fuel versus that required for the most volatile fuel. The Φ vs. injected mass curves for 80°C are very steep, as seen in Figure 3.5. For the case of a hot restart at 80°C, even calibrating with the least volatile fuel would only result in slight overfueling on a mass basis, and the effect on HC emissions would not be as drastic as for colder temperatures. Calibrating for $\Phi = 0.8$ with the High DI fuel at 80°C would result in 8 mg of overfueling for the Base Fuel; by contrast, calibrating with High DI fuel at -6°C would result in 119 mg of overfueling for Fuel #2, the most volatile fuel at cold temperatures. Thus, the effect of fuel properties on first cycle fuel delivery is not as critical for hot restarts as it is for cold or warm starts.

At cold temperatures, very little energy is available to vaporize fuel, either from the port walls or from the fuel itself. Therefore, only the most volatile fuel components are likely to vaporize, and the low end of the distillation curve becomes critical. For -6°C, for example, the best correlation is with T20, however T5 and T10 still have R^2 values greater than 0.9. The very beginning of the distillation curve, the initial boiling point, is not as significant to fuel delivery because these components are highly volatile and thus likely to vaporize under any conditions. This can be seen in Figure 4.5, which shows significant data scatter relative to the linear curve fit.

For each test temperature other than 80°C, there is an optimal distillation point against which to regress, as measured by R^2. As the test temperature increases, this optimal point moves later in the distillation curve, i.e. to higher distillation percentages. Figure 4.18 summarizes these optimal regression points for -6°C, 10°C, 20°C, and 40°C. For the data at 10°C, the best correlation is with T30, however T10 and T20 also give R^2 values greater than 0.9. For the data at 20°C, the best correlation is with T40, and for 40°C, the best correlation is with T50. This explains why the data for 20°C and 40°C correlated well with DI, since the formula for DI is most heavily weighted toward T50.

With higher port wall and fuel temperatures, more total energy in the engine-fuel system is available for vaporization. Therefore, as temperature increases, the less volatile fuel components will be more likely to vaporize and enter the air-fuel mixture. As a future study, this could potentially be verified for the first cycle using gas chromatograph analysis of the trapped air-fuel charge at varying temperatures. The different fuels tested show different fuel delivery behaviors because they have different relative fractions of individual fuel components, and are

thus more or less volatile at different temperatures. This is reflected in the ASTM distillation curves shown in Figure 3.1, where the relative volatilities of the fuels change several times between T10 and T50.

Figure 4.1 – First Cycle Φ vs. Injected Mass at 20°C

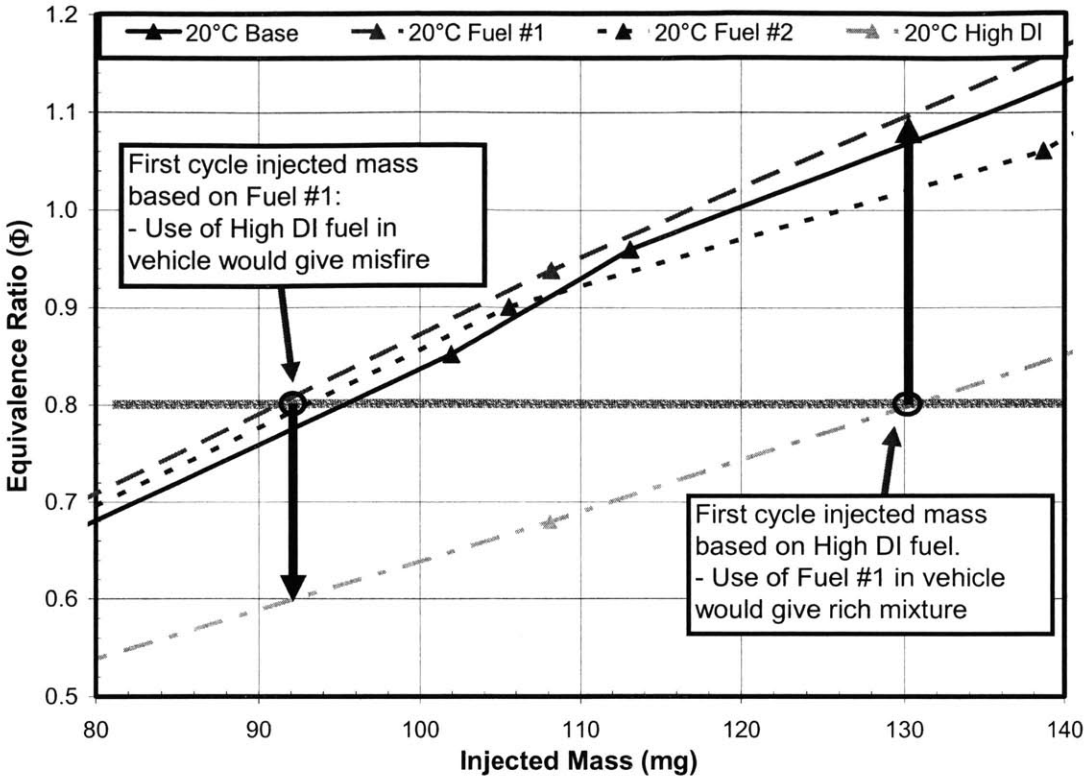

Figure 4.2 – Range of Φ vs. Temperature

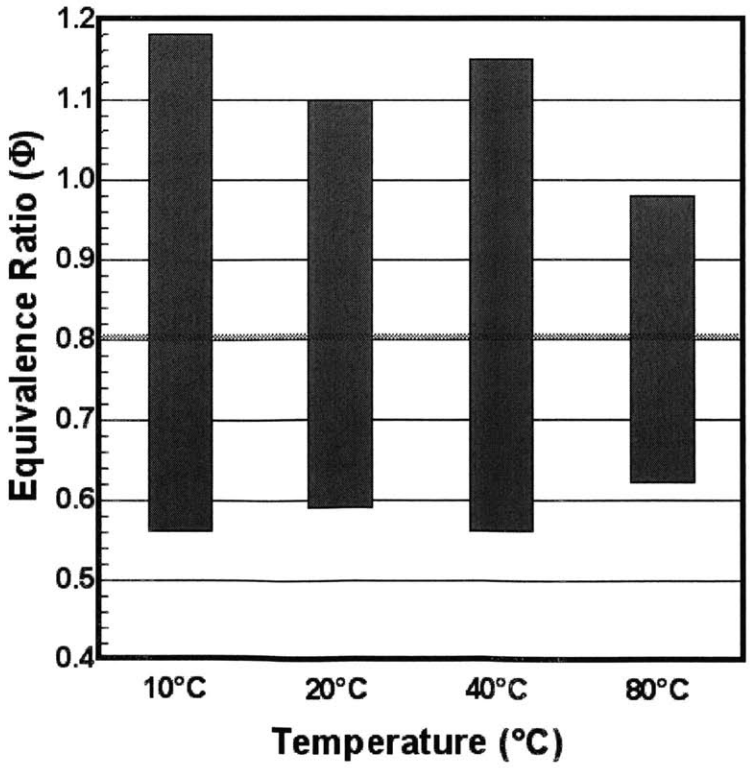

Figure 4.3 – Required Injected Mass vs. DI

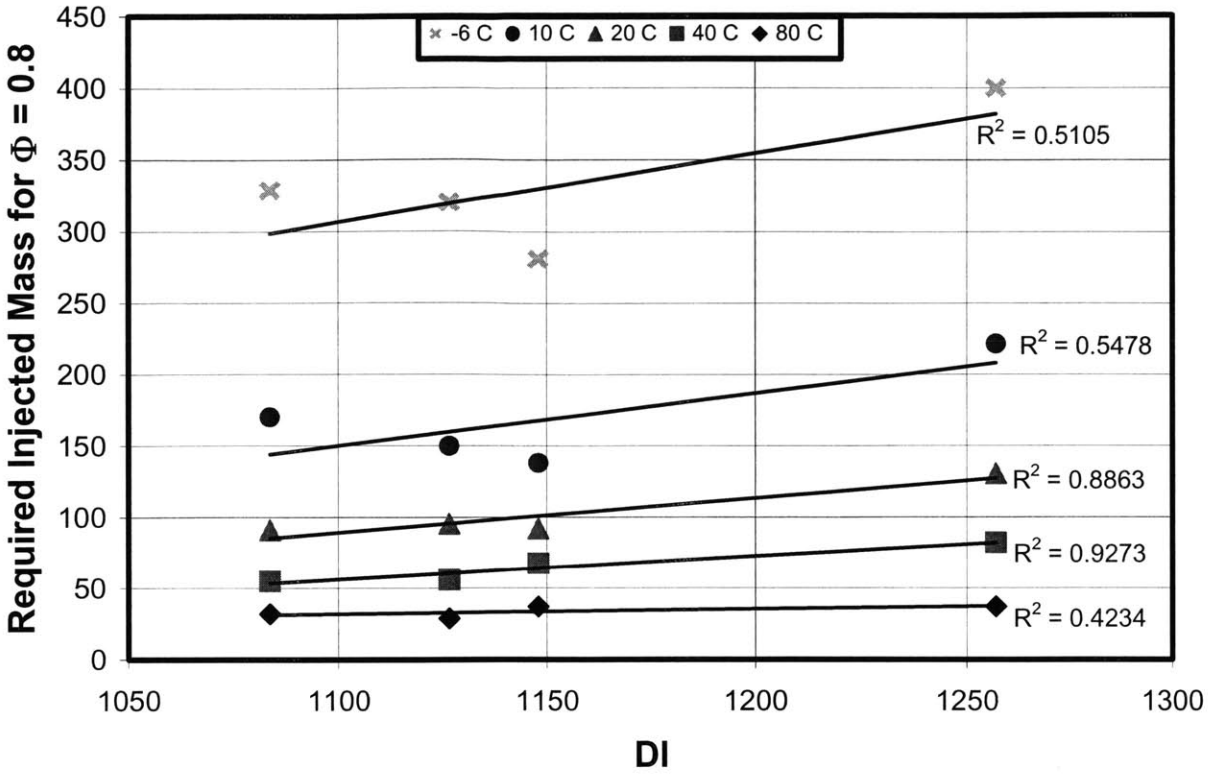

Figure 4.4 – Required Injected Mass vs. RVP

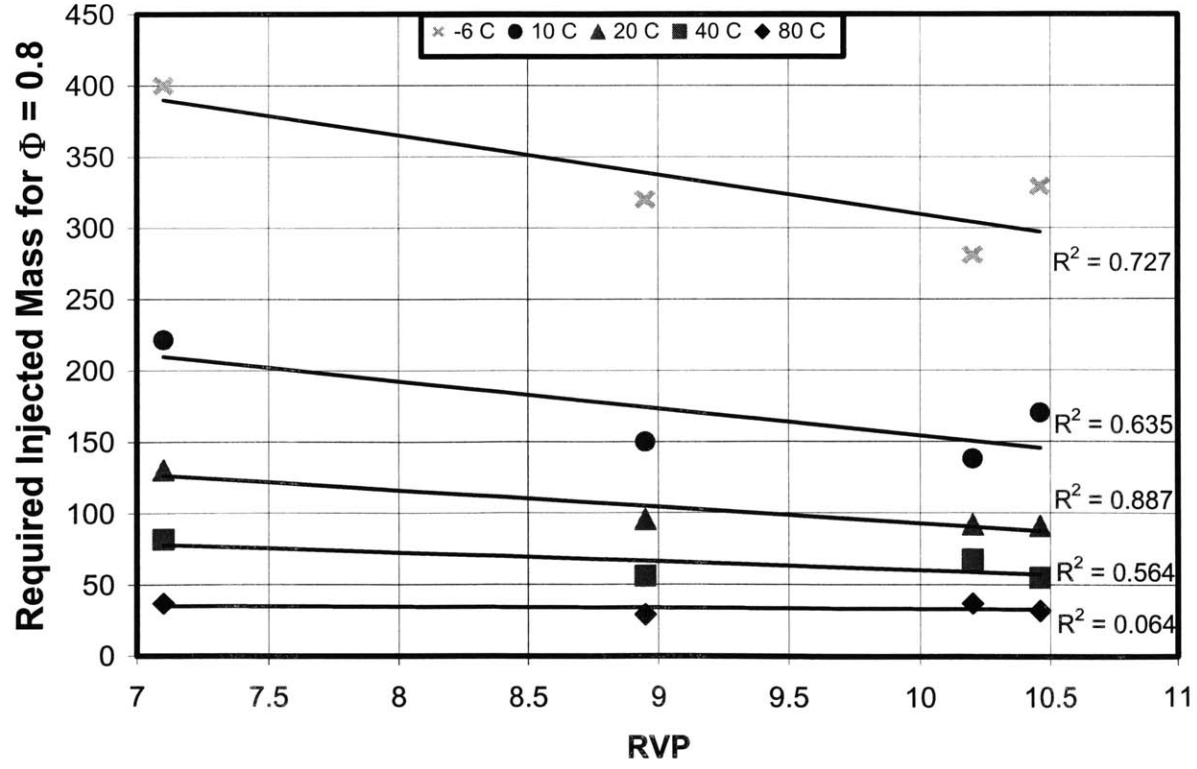

Figure 4.5 – Required Injected Mass vs. Initial Boiling Point

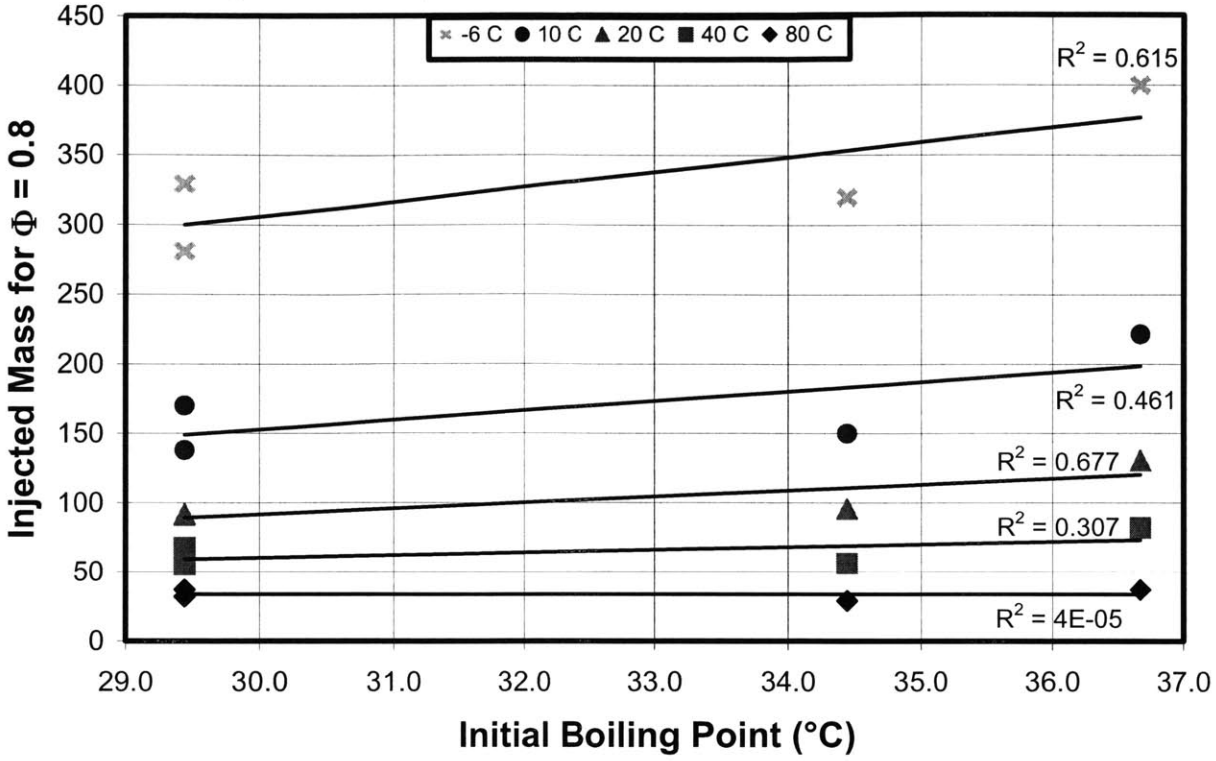

Figure 4.6 – Required Injected Mass vs. T5

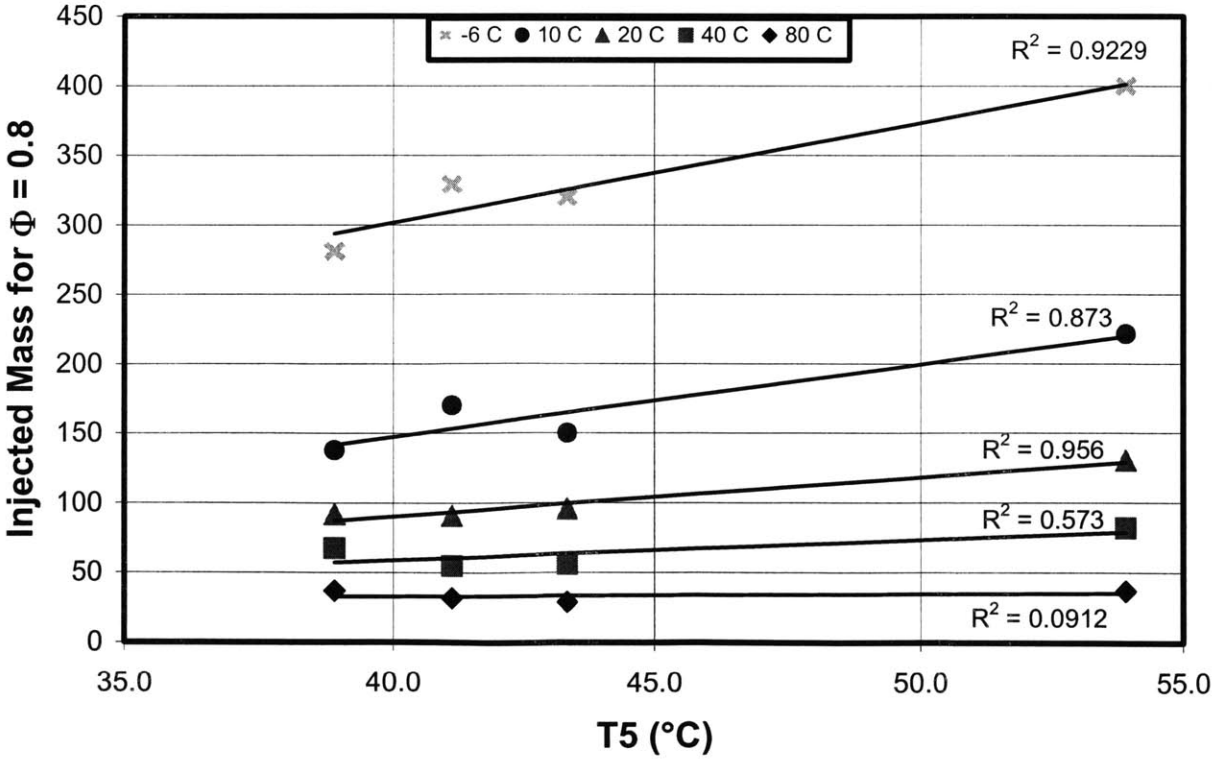

Figure 4.7 – Required Injected Mass vs. T10

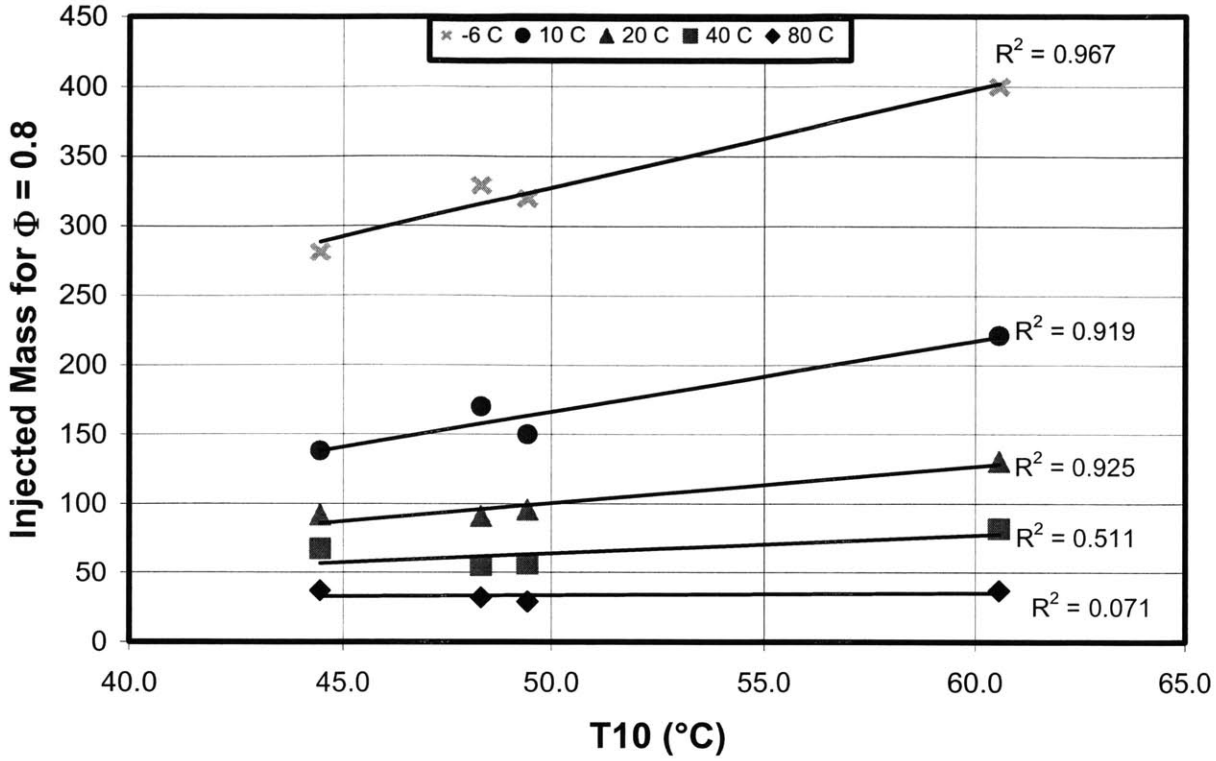

Figure 4.8 – Required Injected Mass vs. T20

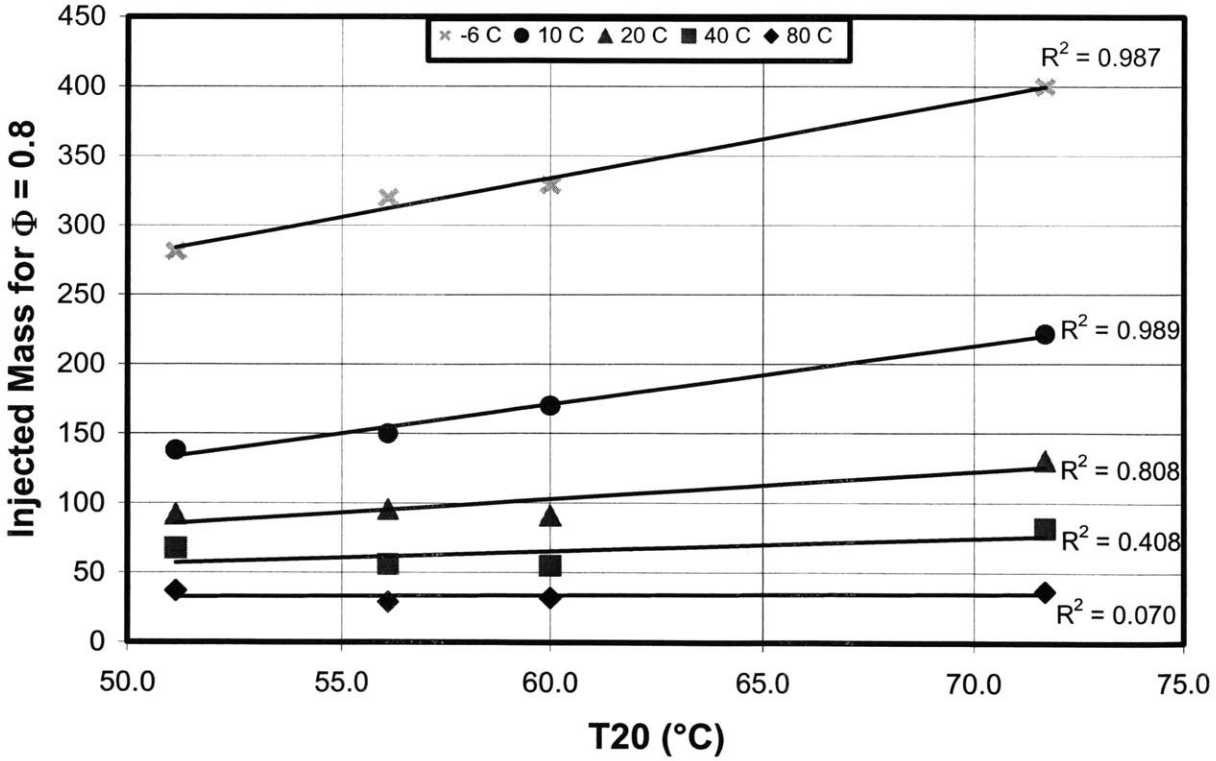

Figure 4.9 – Required Injected Mass vs. T30

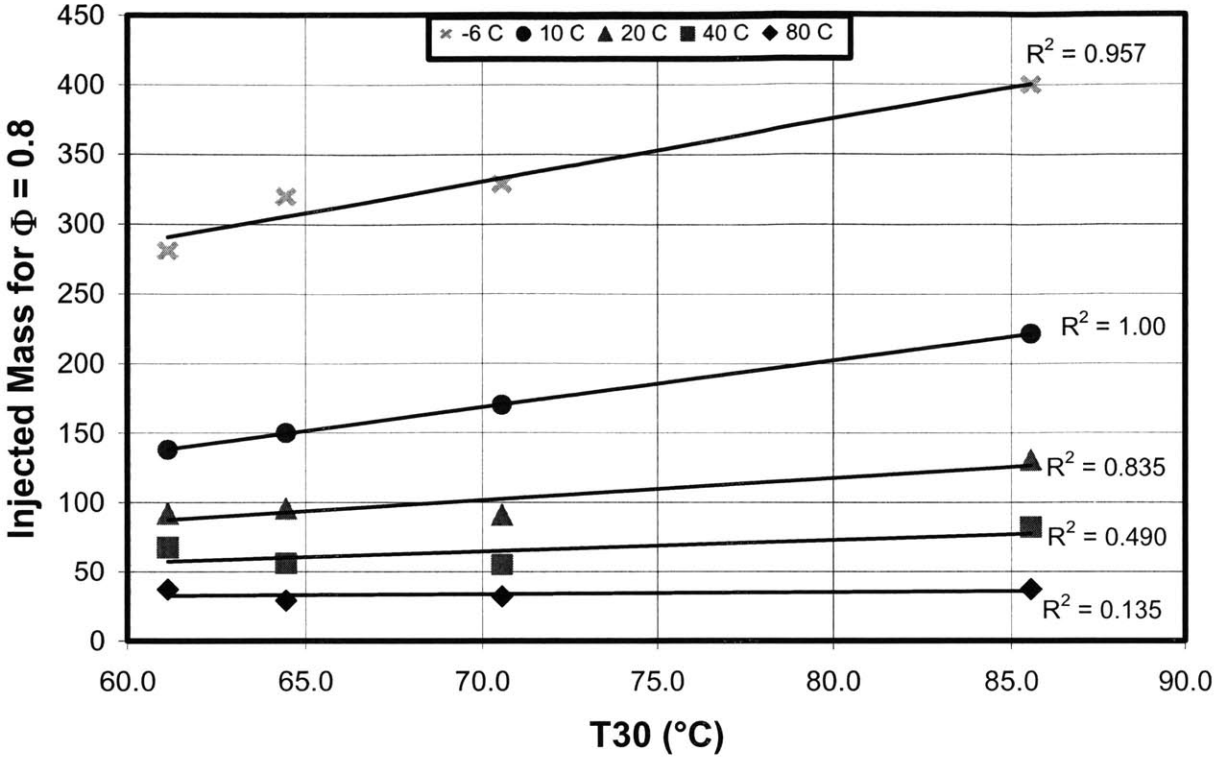

Figure 4.10 – Required Injected Mass vs. T40

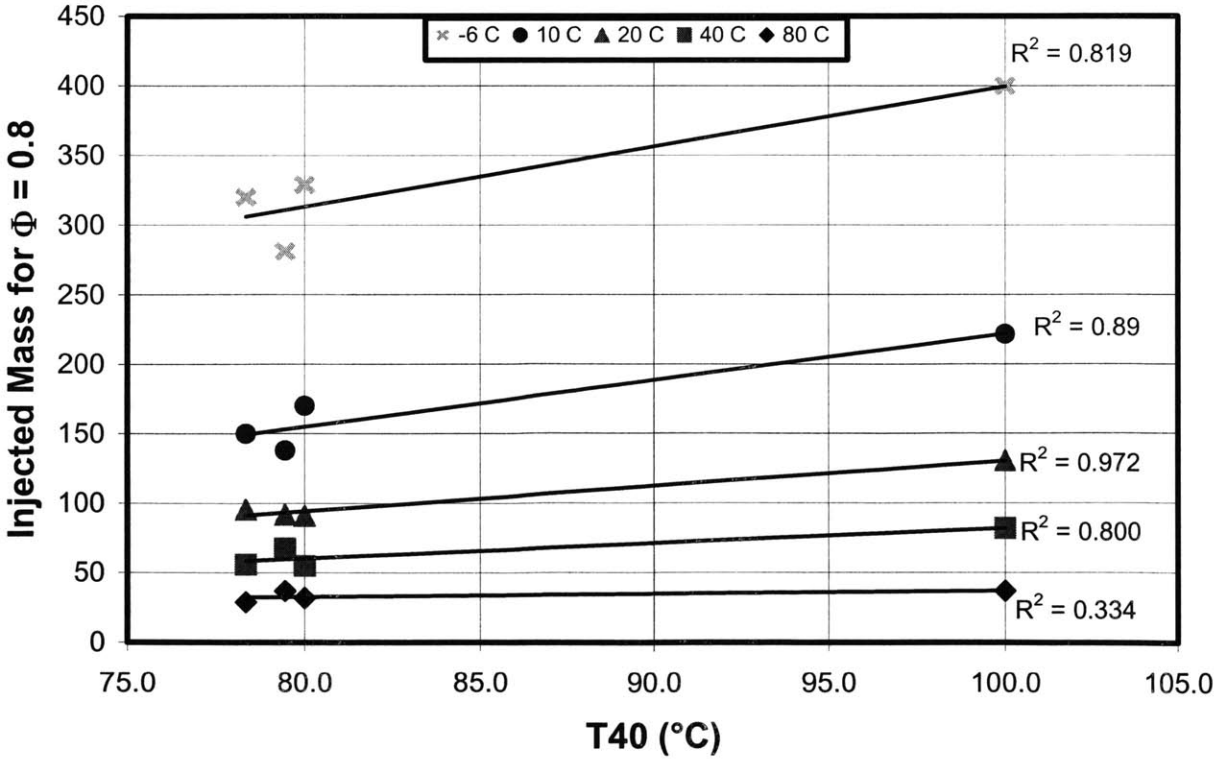

Figure 4.11 – Required Injected Mass vs. T50

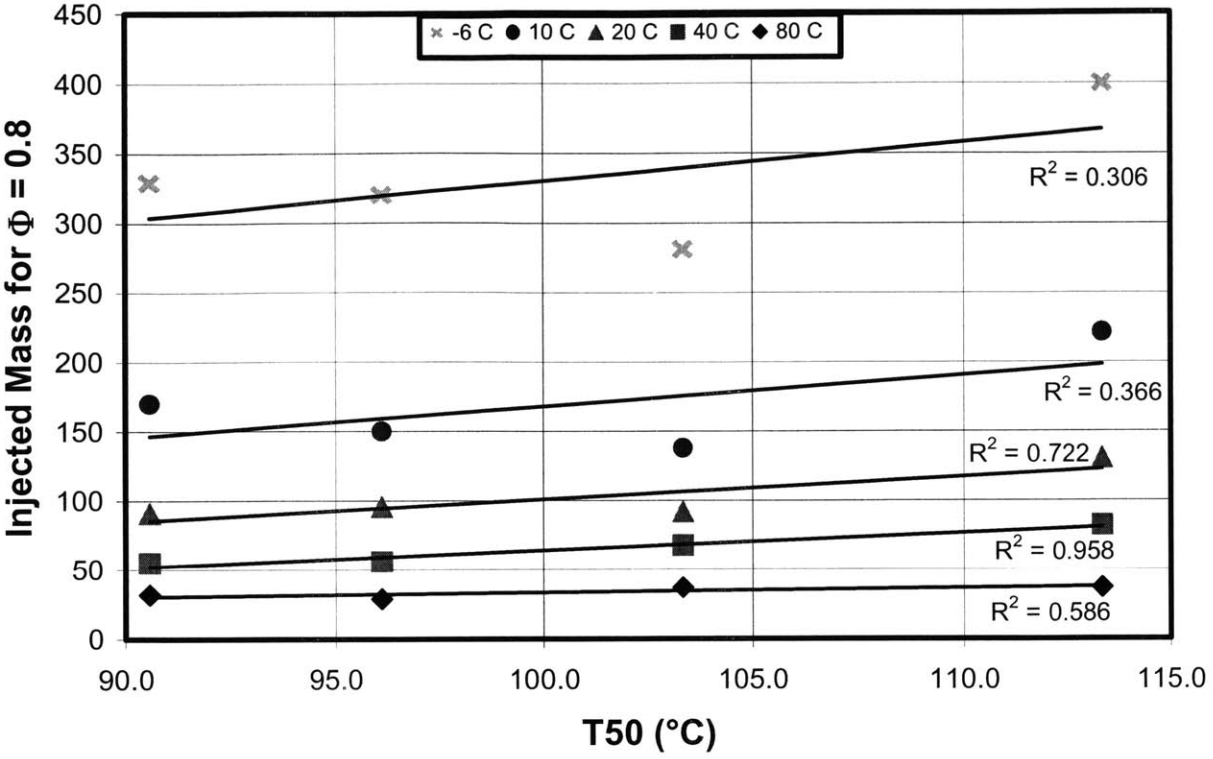

Figure 4.12 – Required Injected Mass vs. T60

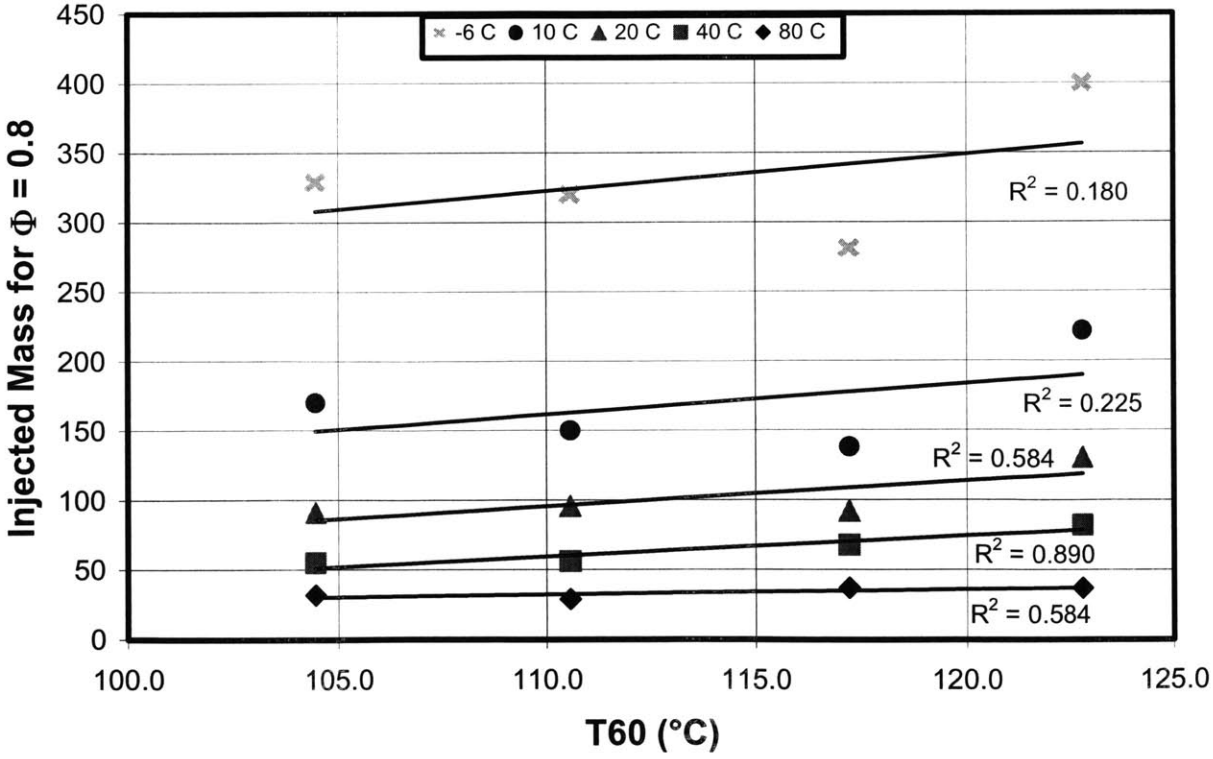

Figure 4.13 – Required Injected Mass vs. T70

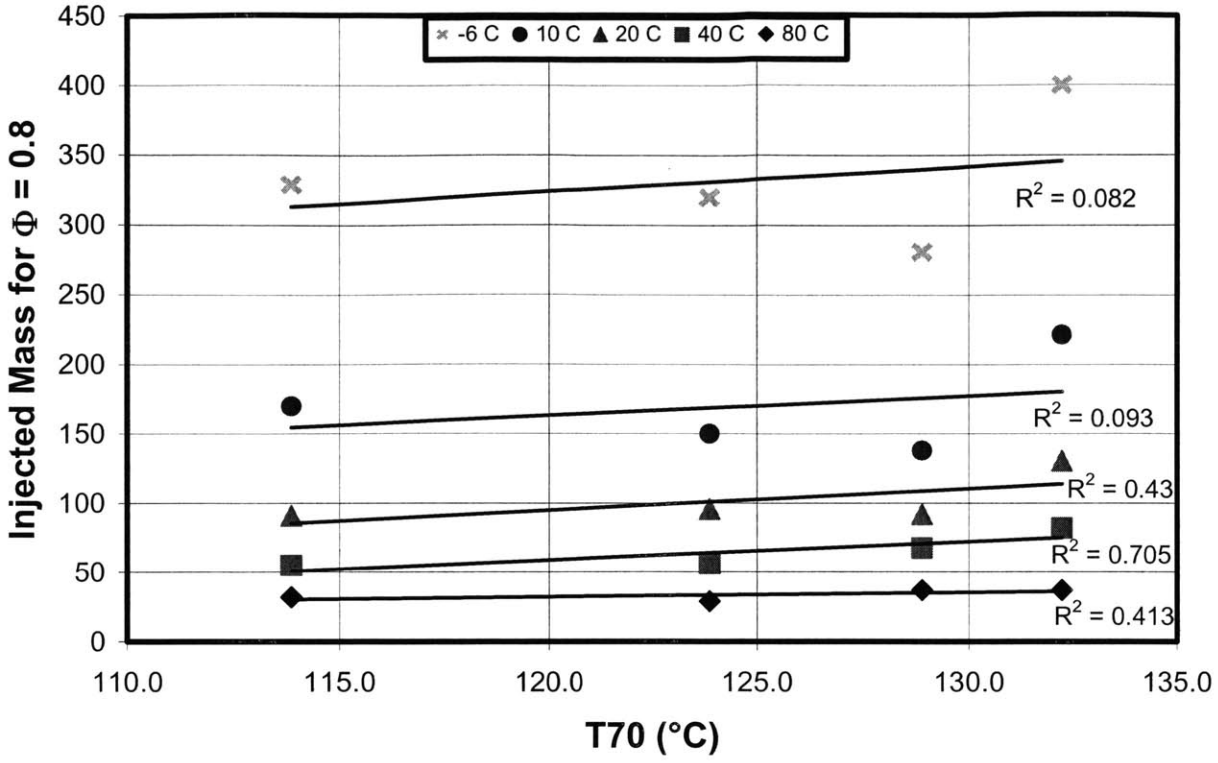

Figure 4.14 – Required Injected Mass vs. T80

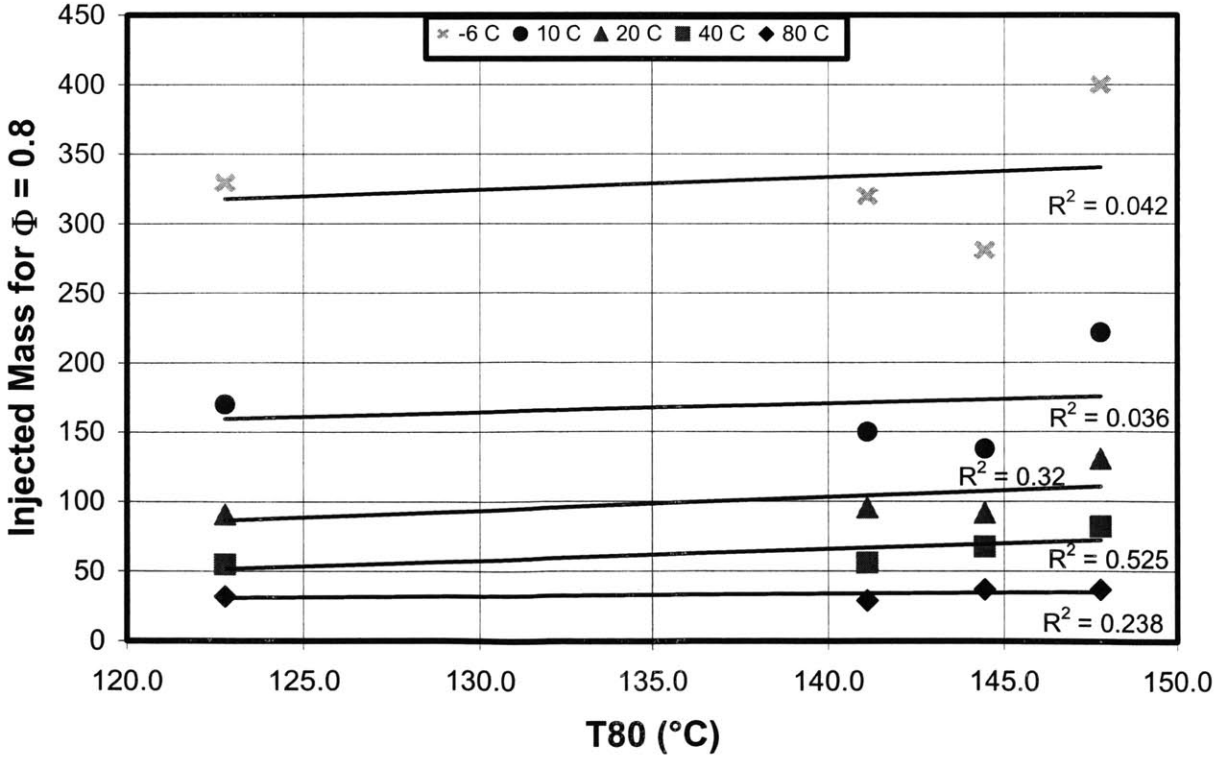

Figure 4.15 – Required Injected Mass vs. T90

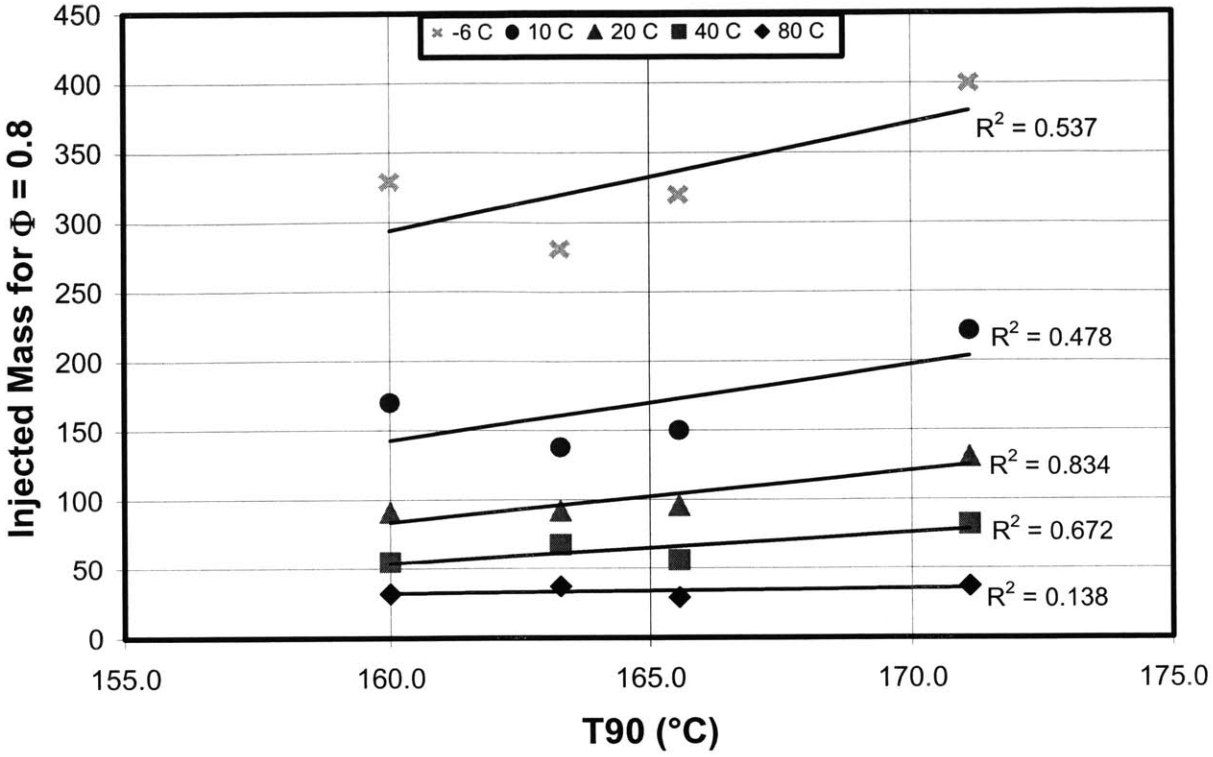

Figure 4.16 – Required Injected Mass vs. T95

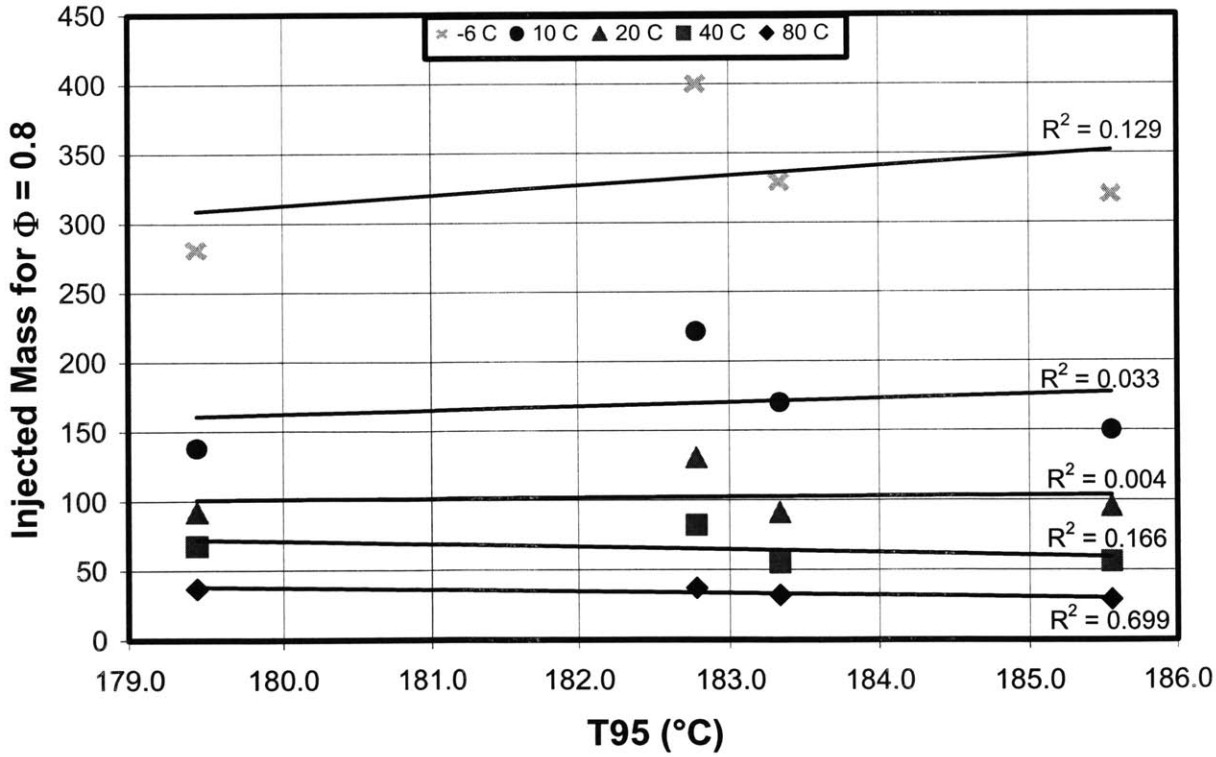

Figure 4.17 – Required Injected Mass vs. End Point

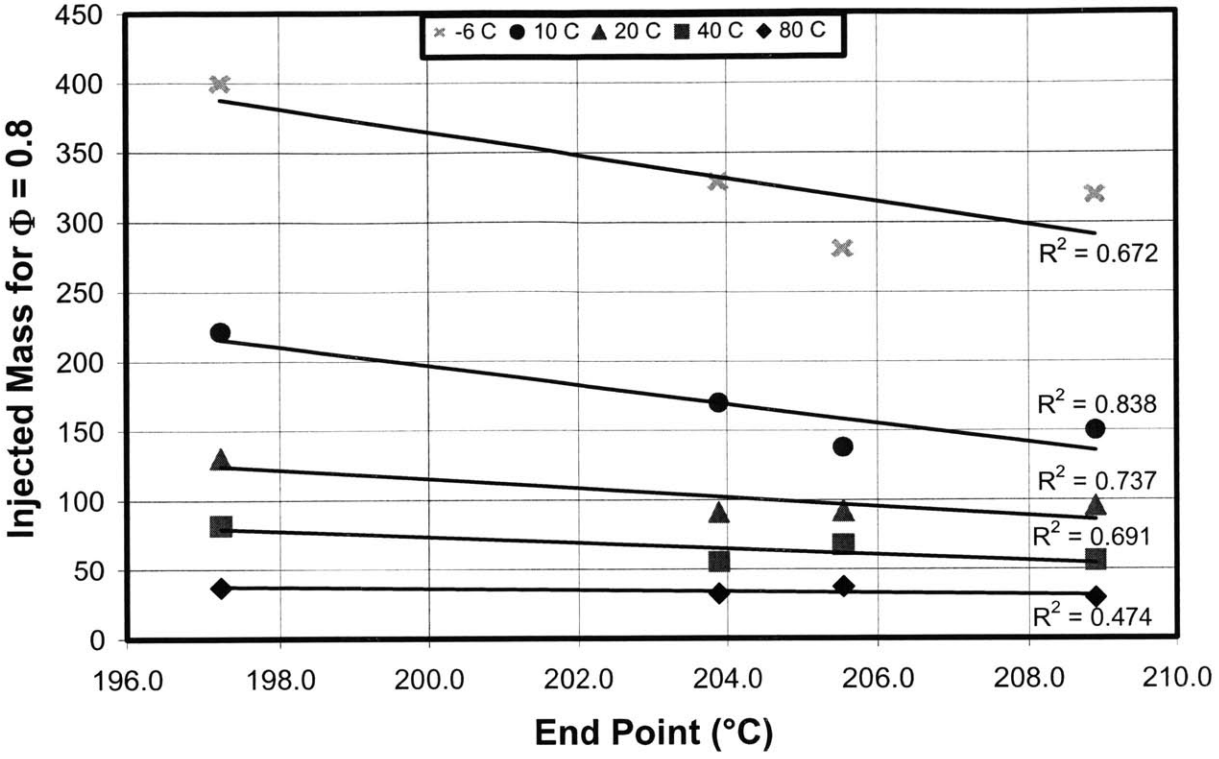

Figure 4.18 – Best Correlations for Required Injected Mass

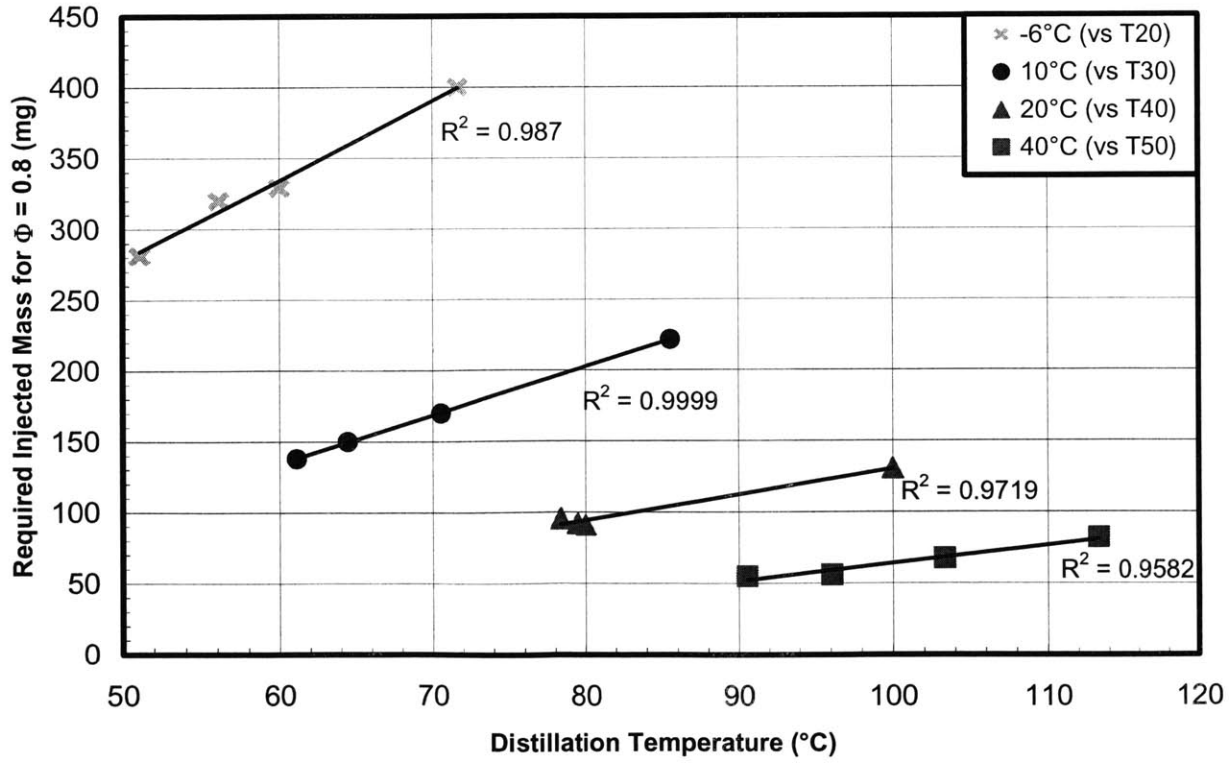

Chapter 5

FUEL DELIVERY MODEL

5.1 Overview of Fuel Delivery Models

Several different approaches have been developed for modeling fuel transport phenomena in PFI engines. The three major methods used to model fuel delivery are the semi-empirical X-τ model, the particle tracking model, and the continuous physical model. [15] The X-τ is the simplest computationally. The X term represents the fraction of injected fuel mass that enters the intake port wall film, with (1-X) thus the fuel that remains airborne and directly enters the air-fuel mixture that enters the cylinder. The τ term is a time constant for fuel film delivery into the cylinder. Both of these values must be determined empirically, as they are unique to each engine and operating conditions due to their dependence on engine geometry and thermal environment. The particle tracking method is considerably more computationally intensive, since it represents the liquid fuel as a collection of droplets and uses Lagrangian methods to track the fuel transport. This is often coupled to a computational fluid dynamics (CFD) code to evaluate the effect of fuel injector spray impingement and surface tension on the wall film. The continual physical model solves the heat transfer and mass transfer simultaneously for the liquid fuel puddles.

In order to assess the effect of fuel properties on first cycle fuel delivery using a model, said model must represent the unique composition of each fuel. While a generic fuel input might be useful for modeling wall film dynamics or injector effects, for the purpose of this study the fuel itself must be accurately modeled before applying a fuel delivery model. Two previously developed models, one for modeling the ASTM D86 distillation curve and the other for modeling fuel delivery, were adapted to capture the effects of fuel properties.

5.2 Distillation Curve Model

5.2.1 Overview

To model the evaporation and mixing of liquid fuel into air, the thermo-physical properties of the fuel must be accurately represented. Typical gasoline fuels contain more than 100 different HC species, and the thermodynamic properties and species-to-species interactions are not well known for many of these species. However, an accurate fuel model must still

contain several different HC species to capture the effect of the light components evaporating before the heavier components, as seen in the ASTM distillation curve. Thus, a simplified representation of the fuel must be used.

The major-component fuel model developed in [16] represents gasoline by grouping the HC species according to the number of carbon atoms in the molecule and by the molecular structure, e.g. paraffins, olefins, aromatics. Table 5.1 lists the components used in the model, which include MTBE since the model was originally developed for use with oxygenated fuels. For each grouping, the most abundant species takes on the weight percentage of the entire group, and the thermo-physical properties for the group are assumed to be those for the major species. The major-component model has been previously demonstrated to accurately match the ASTM distillation curve and RVP, given a known fuel composition consisting only of components that are captured in the model.

5.2.2 Distillation Curve Model Results

This study represents a new application of the major-component fuel model. Rather than modeling the ASTM distillation curve based on a known fuel composition, the unknown fuel compositions were modeled based on known distillation curves. The exact chemical composition of each fuel was not known, but the distillation curves were available. (See Figure 3.1.) Thus, to determine an approximate composition for each fuel using the major-component representation, the relative fractions of each component in the model were adjusted to match the simulated distillation curve to the measured distillation curve. Table 5.2 shows the component mole fractions for each of the simulated fuels. Note that none of the fuels are oxygenated, thus MTBE is zero for each. Additionally, not all components were used for each of the fuels. This may or may not accurately reflect the exact composition of the fuels, but leaving out some species was necessary to closely match the distillation curves.

The simulated distillation curves for each of the four fuels closely match the test data, as shown in Figures 5.1 –5.4. As found in previous studies ([12], [16]), the initial boiling point and end point are the most difficult to accurately capture with the model. Nonetheless, based on this simulation, the fuel models are assumed to closely capture the thermo-physical behavior of the actual fuels, such that the model components could be used as inputs to a fuel delivery model.

5.3 Fuel Delivery Model

5.3.1 Overview

First cycle fuel delivery is a complex, non-equilibrium process involving evaporation and mass transport of a multi-component substance. To capture this process in a sufficiently simple manner, a modified version of the mixture preparation model developed by Santoso and Cheng in [17] is used. The distribution of fuel vapor in an air-fuel mixture can be described by a probability density function (PDF), which indicates the probability of the presence of a given air mass fraction in each mass element of air-fuel charge. To accurately find the PDF requires detailed modeling of the fuel delivery process, including injection, wall film dynamics, evaporation, and mixing. This PDF representation can be simplified, however, by assuming that the available air in the port can be separated into two categories: the fraction of air that interacts with liquid fuel, and the fraction that does not. The fraction of air that interacts with fuel can then be assumed to reach thermal equilibrium with fuel, and subsequently the fuel mass is divided into vapor and liquid phases.

This partial equilibrium approximation is illustrated in Figure 5.5. In the top diagram, the mass elements with $Y_a = 0$ contain only pure fuel, either in liquid or vapor form, the mass elements with $Y_a = 1$ have only pure air, and mass elements with $0 < Y_a < 1$ contain a mixture of air and fuel. In the bottom diagram, the mass elements with non-zero fuel vapor fraction, including the pure fuel vapor, are lumped together into one element, which is assumed to be in thermal equilibrium with the liquid fuel in the charge. Thus, only part of the charge air is assumed to be in thermodynamic equilibrium with the fuel.

The model does not specify the physical location of the mass elements, but rather assumes that all fuel vapor goes into the combustible mixture; the location of the liquid fuel is not explicitly specified. To determine the correct amount of fuel vapor based on thermodynamic equilibrium, the mass of air that equilibrates with the fuel must be determined. This mass is described physically as the mass of air in the boundary layer between the liquid fuel and the pure air. This should be proportional to $(\rho_a)(D)(t)(Sh)$: D is the mass diffusivity, which should scale as $T^{3/2}/P$; the diffusion time scale t scales as 1/RPM; and the Sherwood number Sh is assumed to be constant. Introducing some normalizing values for temperature and RPM, the equilibrated air mass is calculated using the following expression.

$$m_a = 0.05\sqrt{\frac{1000}{RPM}}\frac{MAP^{0.5}}{(T/300)^{0.25}}$$

The exact value of the proportionality constant was set to match the model to the experimental data.

Using the approximated fuel composition determined by the distillation curve model described above, the thermophysical properties of the fuel were calculated using the NIST database, as described in [17]. These properties are then used to perform a modified isothermal flash boiling calculation for the mass of injected fuel specified and the mass of air in equilibrium, at the given ECT and MAP. This calculation was modified from the original model to better match experimental data. An additional parameter was included to adjust the fraction of the heat of vaporization supplied by the port walls, as a function of injected mass. As more fuel is injected, the relative fraction of fuel mass that evaporates in-flight will be lower, and thus more energy must be supplied externally to vaporize the fuel. Thus, this function approaches zero at low values of injected mass, and unity at high values of injected mass. The specific shape of this function was set in order to match the model output to experimental data for each of the four fuels as closely as possible. The original model developed in [17] was calibrated for only one fuel, which contained MTBE, and thus needed to be modified for the non-oxygenated fuels used in this study. The fraction f of the heat of vaporization that is supplied externally was represented as follows.

$$f = 1 - \exp\left(-\frac{m_{inj} - 0.03}{0.10}\right)$$

Several features of the model should be noted. First, the model does not contain any information regarding fuel spray pattern or port geometry, and thus the model must be calibrated using the expressions for m_a and f to make it engine-specific. Second, m_a is assumed to be independent of m_{inj} for a fixed port geometry and injector spray patter, since typical fuel droplets from the injector are greater than 100 μm in diameter and thus almost all are deposited on the port wall.

The only model inputs are thus injected fuel mass, ECT, MAP, engine speed (RPM), and the fuel composition represented as described above.

5.3.2 Fuel Delivery Model Results

To simulate first cycle fuel delivery using the model, input parameters were matched to actual engine conditions for RPM, MAP, and the range of injected fuel mass. As shown in Figure 5.6, overall the model agrees quite well with the experimental data across a wide range of ECT and injected mass, and for each of the four fuels. The model parameters m_a and f were calibrated only using data for the Base Fuel, and the model was then run for each of the other fuels with no further modifications.

Figures 5.7 – 5.10 show the predicted Φ vs. injected mass for each of the four fuels. In general the model agrees well with experimental data, but at very high injected mass the model predicts significantly lower Φ than was observed in testing. The model also under-predicted Φ for very cold temperatures, and thus did not predict combustible mixtures for some of the fuels at -6°C. However, the model agreement is generally good in the range of injected mass that would be of interest in engine development, for temperatures greater than or equal to 10°C. Figure 5.11 compares the model's prediction for the required injected mass to achieve $\Phi = 0.8$ to the value determined experimentally. While the general trends as a function of ECT are closely matched, the small differences between fuels are not captured as accurately. This could be attributable to the fuel model, which might not model the subtle differences in distillation properties as closely as necessary. The trends in fuel delivery behavior of the High DI fuel compared to the other fuels are closely matched, but the High DI fuel has a substantially different distillation curve than the other fuels. At 20°C, the percent difference between the Base Fuel and Fuels #1 and #2 is very small even for the experimental data, and the model is not sophisticated enough to accurately capture those differences.

Thus, the partial air equilibrium fuel delivery model can predict overall trends in fuel delivery based on ECT, but it does not have sufficiently high resolution to distinguish between fuels with very similar distillation curves.

Table 5.1 – Chemical Species Used in Major-Component Model

Carbon Structure	Description	Most Abundant Species	Model Name	Density (mole/L)	Normal Boiling Point (°C)
C4	Paraffins+olefins	n-Butane	'c4'	9.940	-0.6
C5	Paraffins+olefins	Iso-Pentane	'ic5'	8.597	28.0
MTBE	Oxygenate	MTBE	'mtbe'	8.440	55.0
C6	Paraffins+olefins	Iso-Hexane	'ic6'	7.568	60.2
AC6	Aromatics	Benzene	'bnz'	11.195	80.1
C7	Paraffins+olefins	2,3-Dimethyl Pentane	'23dmp'	6.987	90.0
C8	Paraffins+olefins	2,2,4-Trimethyl Pentane	'224tmp'	6.051	99.3
AC7	Aromatics	Toluene	'tol'	9.444	110.8
C9	Paraffins+olefins	3,5-Dimethyl Heptane	'22dmc7'	5.548	133.0
AC8	Aromatics	m-Xylene	'mxyl'	8.194	139.3
AC9	Aromatics	1-Methyl 3-Ethyl Benzene	'cumene'	7.197	152.5
C10	Paraffins+olefins	4-Methyl Nonane	'c10'	5.185	174.0
AC10+	Aromatics	1,2-Diethyl Benzene	'ic4bnz'	6.381	174.0
C11	Paraffins+olefins	n-Undecane	'c11'	4.787	194.5
C12+	Paraffins+olefins	n-Dodecane	'c12'	4.453	214.5

Table 5.2 – Component Mole Fractions for Simulated Fuels

		Fuel Component Mole Fractions			
Carbon Structure	Description	Base	Fuel #1	Fuel #2	High DI
C4	Paraffins+olefins	0.000	0.000	0.000	0.000
C5	Paraffins+olefins	0.378	0.358	0.477	0.212
MTBE	Oxygenate	0.000	0.000	0.000	0.000
C6	Paraffins+olefins	0.123	0.114	0.000	0.217
AC6	Aromatics	0.000	0.000	0.000	0.000
C7	Paraffins+olefins	0.054	0.058	0.000	0.000
C8	Paraffins+olefins	0.095	0.114	0.106	0.059
AC7	Aromatics	0.109	0.228	0.167	0.219
C9	Paraffins+olefins	0.040	0.046	0.054	0.181
AC8	Aromatics	0.076	0.000	0.081	0.000
AC9	Aromatics	0.035	0.000	0.027	0.000
C10	Paraffins+olefins	0.011	0.000	0.007	0.015
AC10+	Aromatics	0.035	0.035	0.034	0.022
C11	Paraffins+olefins	0.026	0.035	0.034	0.074
C12+	Paraffins+olefins	0.016	0.011	0.014	0.000

Figure 5.1 – Simulated vs. Actual Distillation Curve for Base Fuel

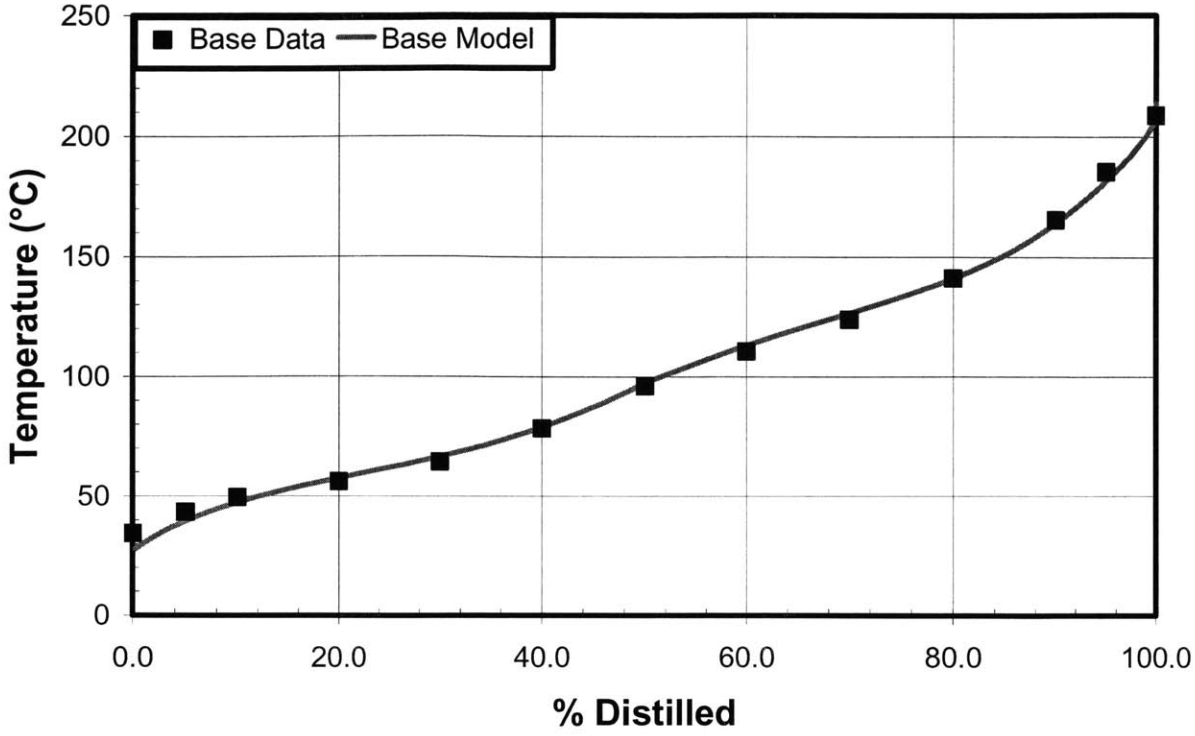

Figure 5.2 – Simulated vs. Actual Distillation Curve for Fuel #1

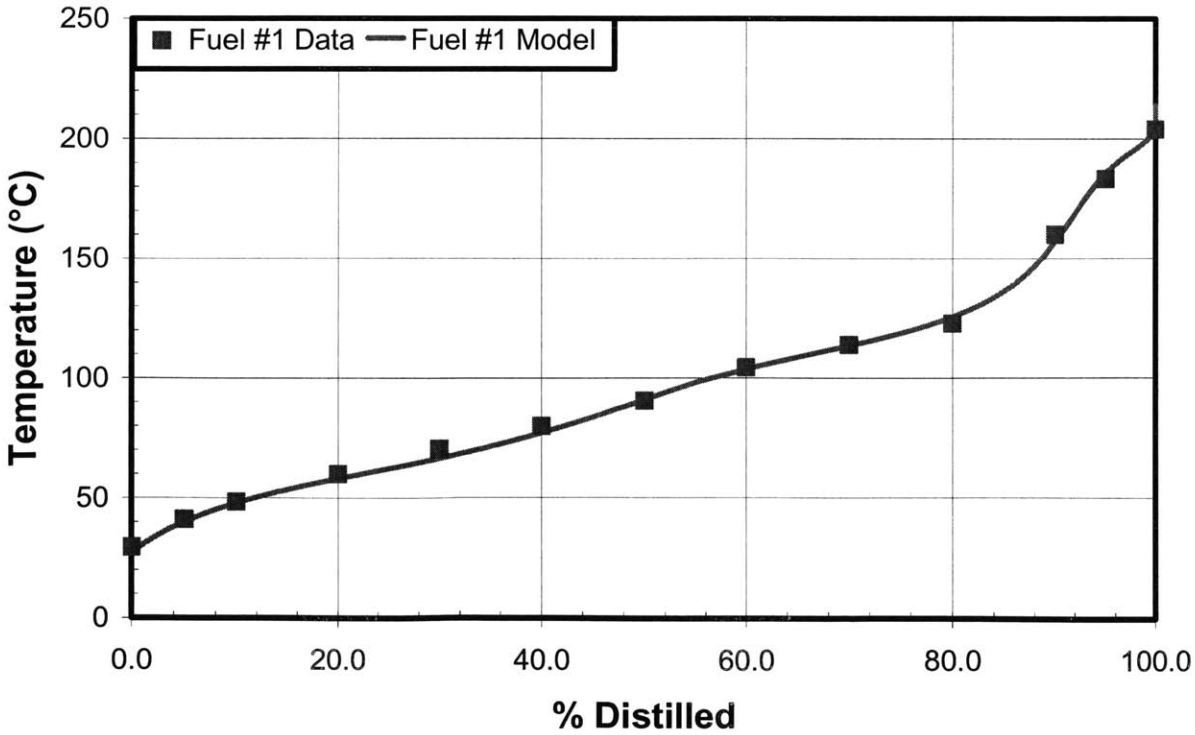

Figure 5.3 – Simulated vs. Actual Distillation Curve for Fuel #2

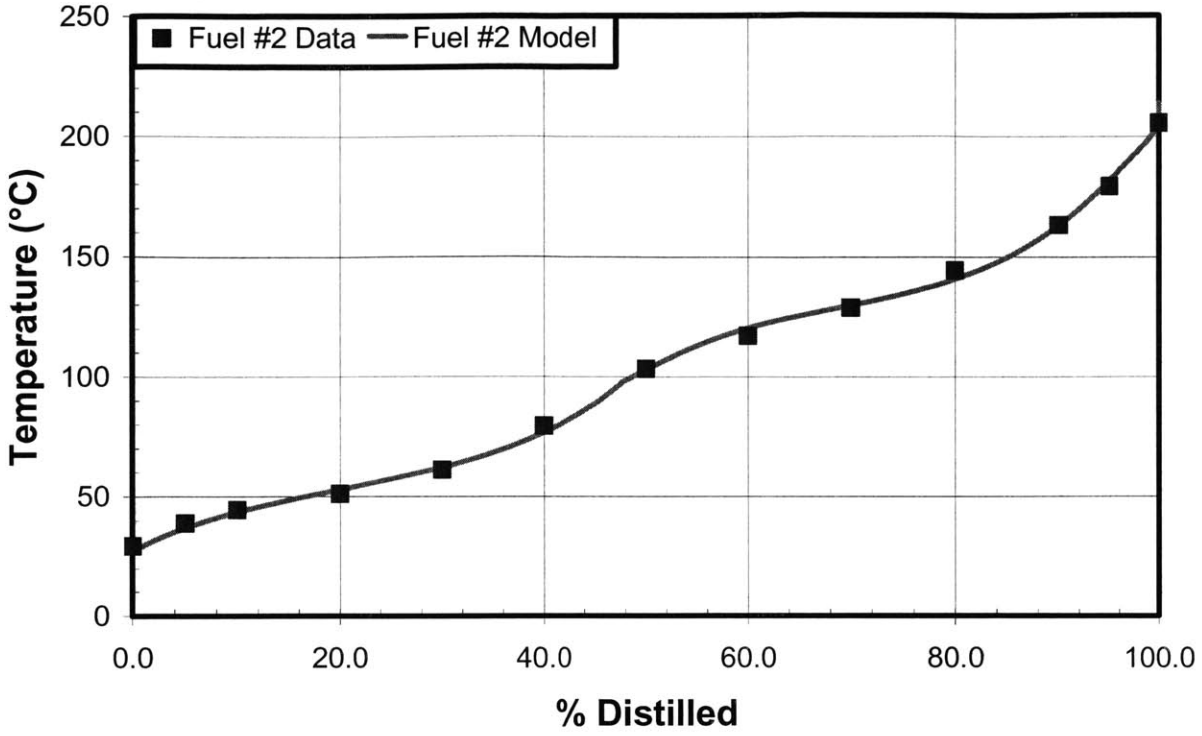

Figure 5.4 – Simulated vs. Actual Distillation Curve for High DI Fuel

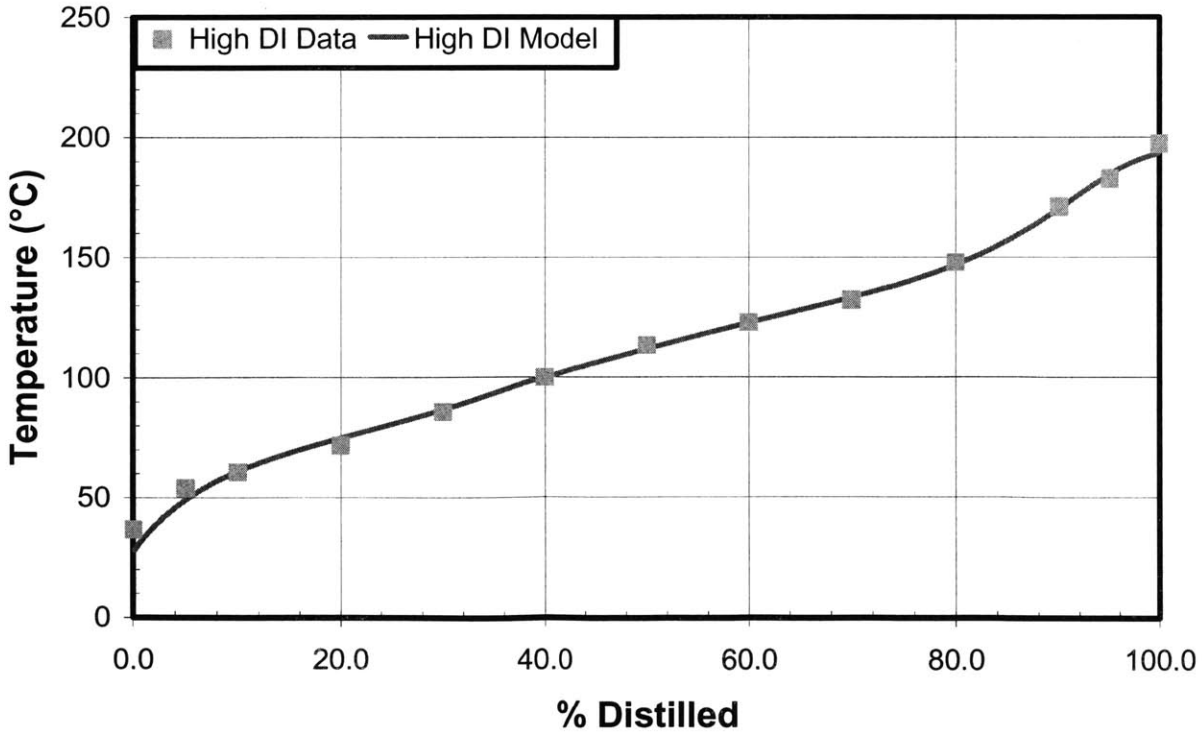

Figure 5.5 – Concept of Fuel Delivery Model
Based on Effectively Equilibrated Air Mass Fraction

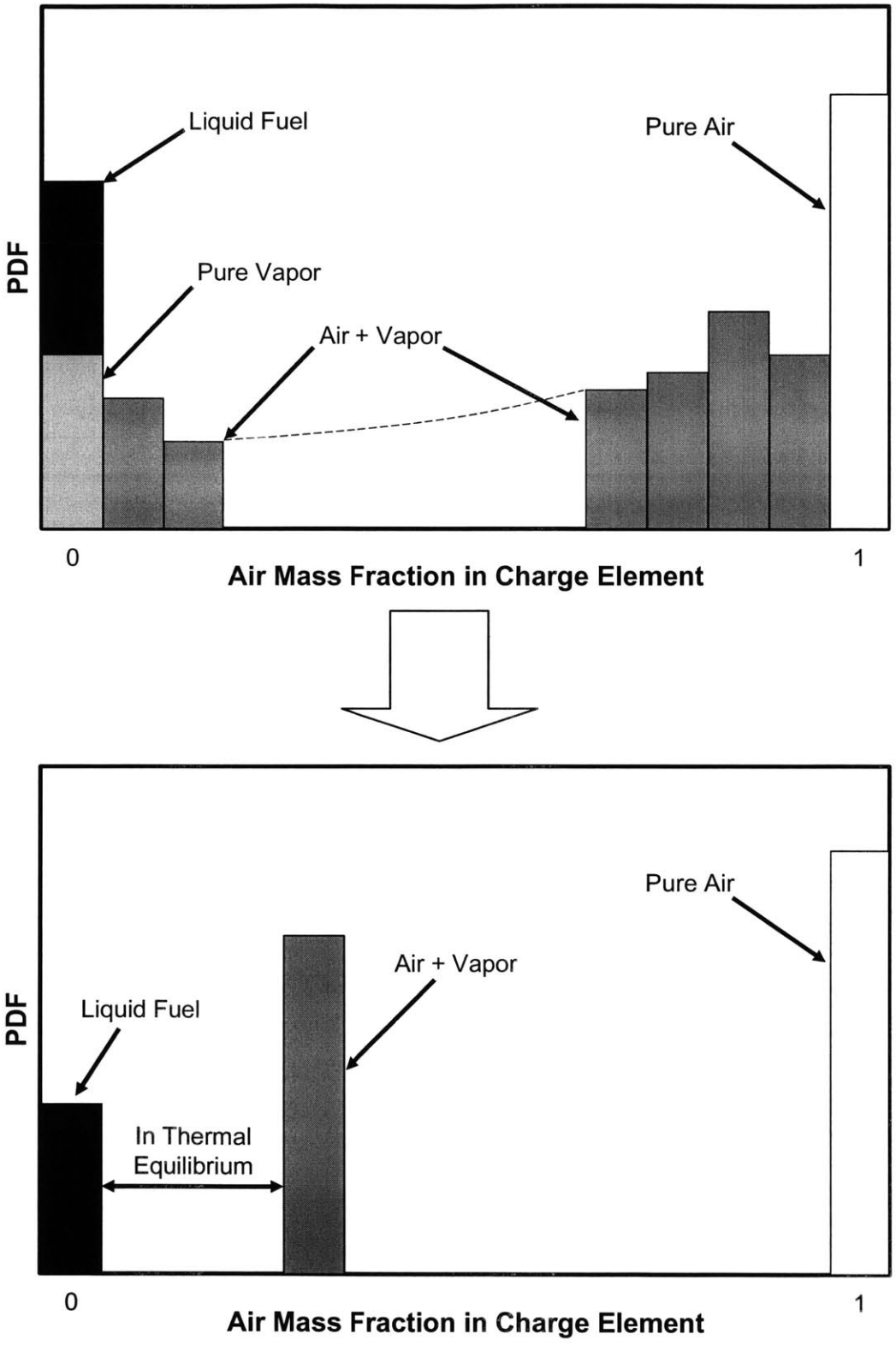

Figure 5.6 – Comparison of Fuel Delivery Fraction from Model vs. Data

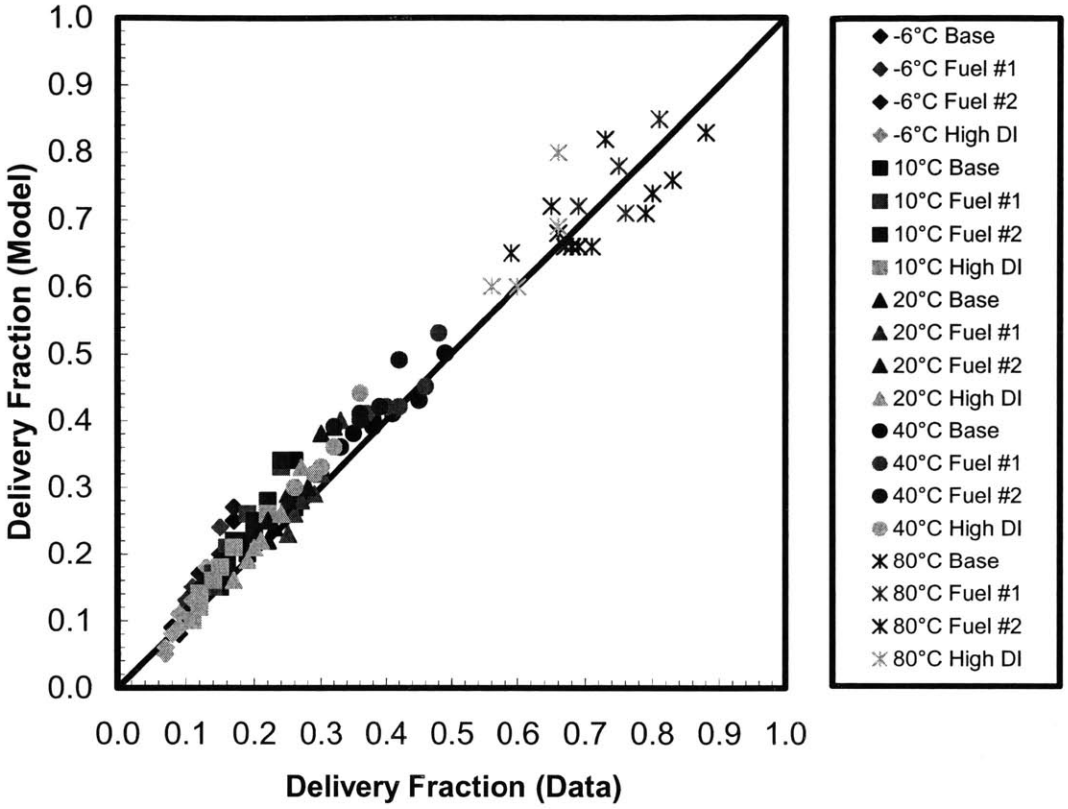

Figure 5.7 – Comparison of Φ vs. Injected Mass for Model & Data, Base Fuel

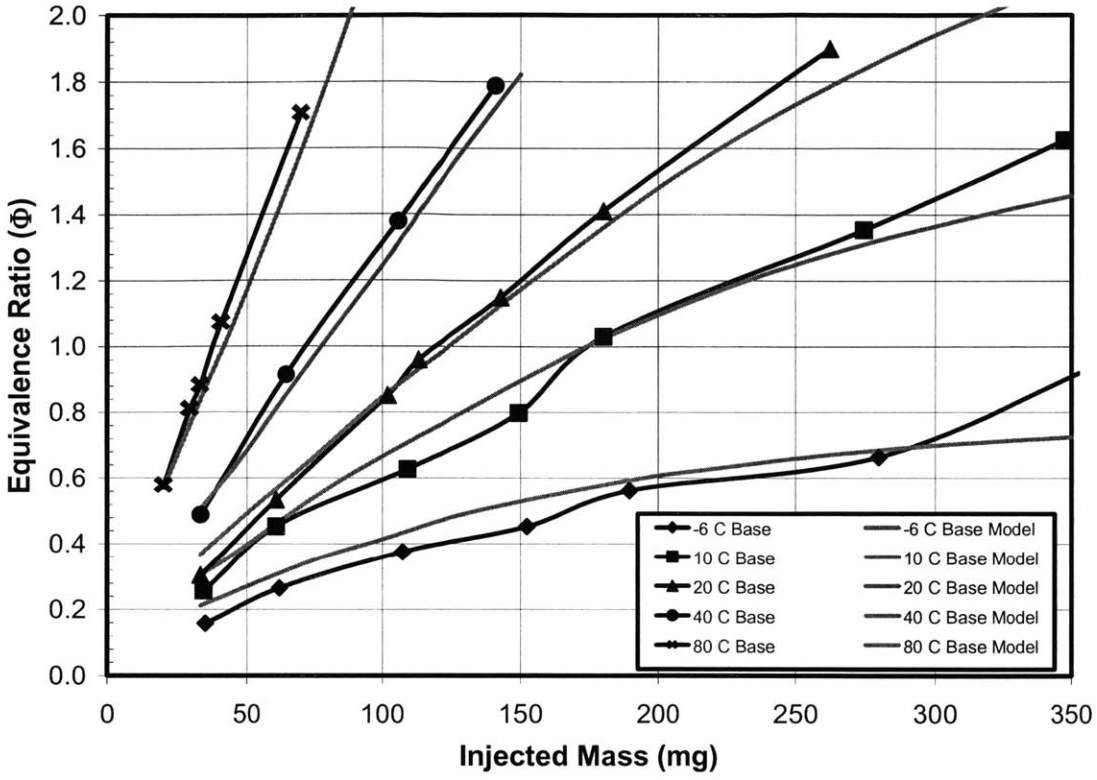

Figure 5.8 – Comparison of Φ vs. Injected Mass for Model & Data, Fuel #1

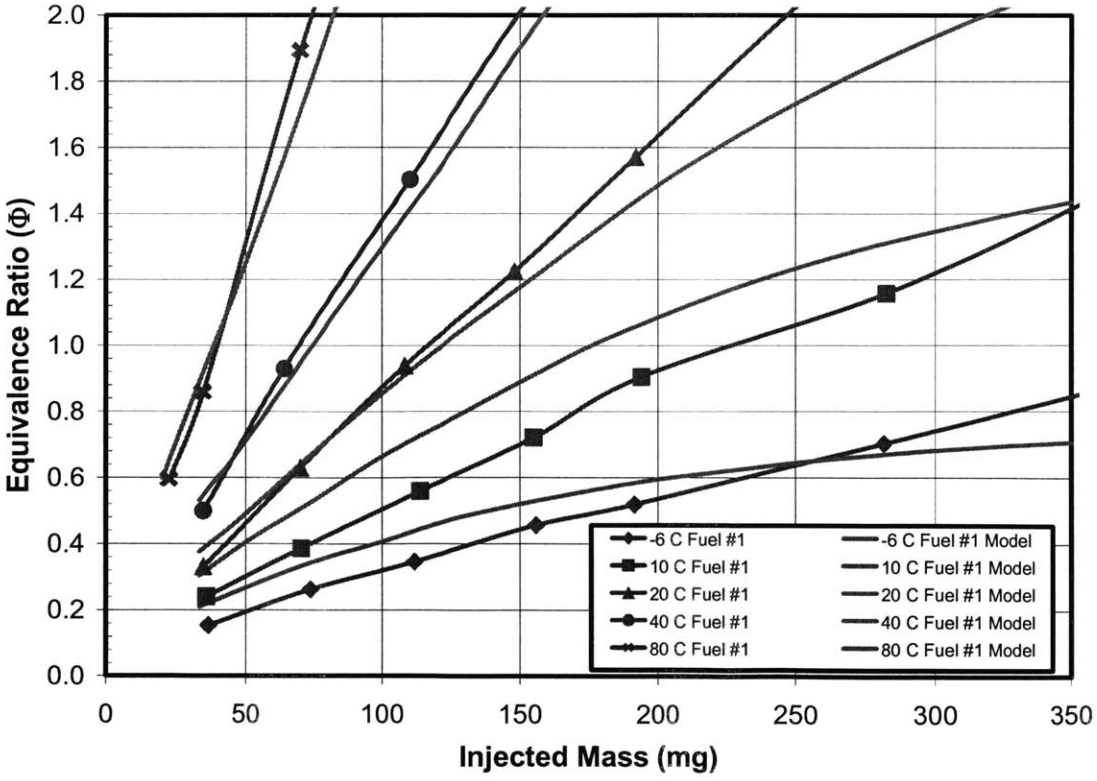

Figure 5.9 – Comparison of Φ vs. Injected Mass for Model & Data, Fuel #2

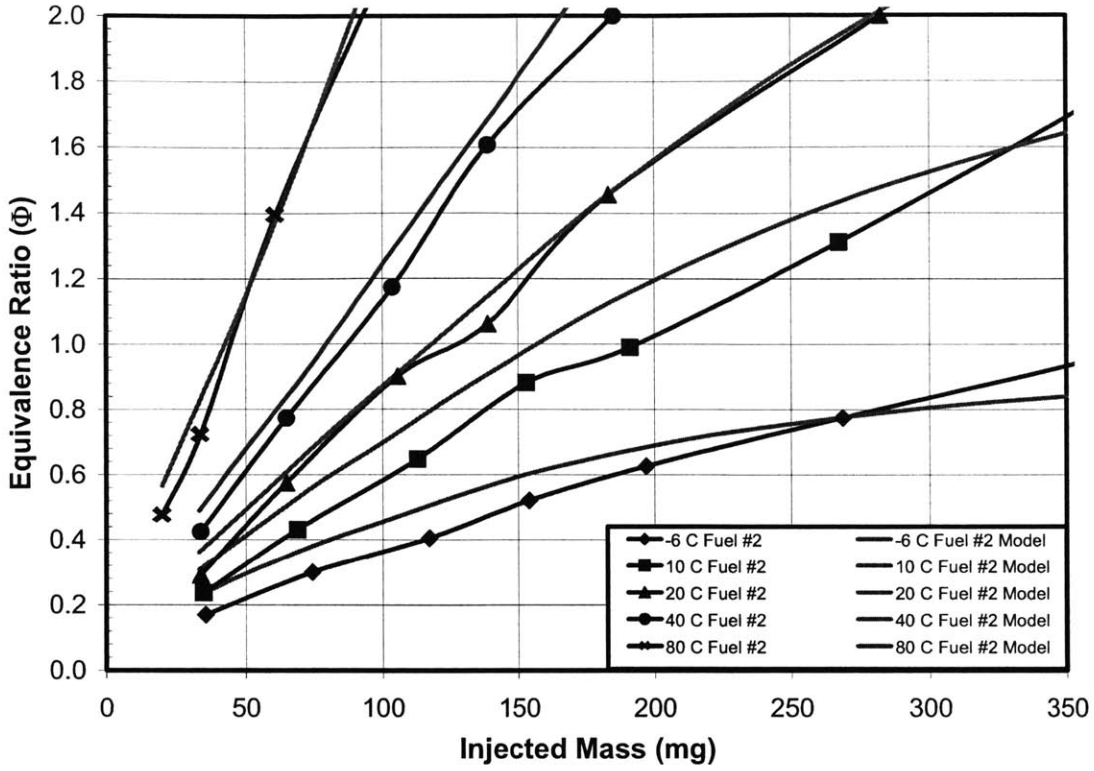

Figure 5.10 – Comparison of Φ vs. Injected Mass for Model & Data, High DI Fuel

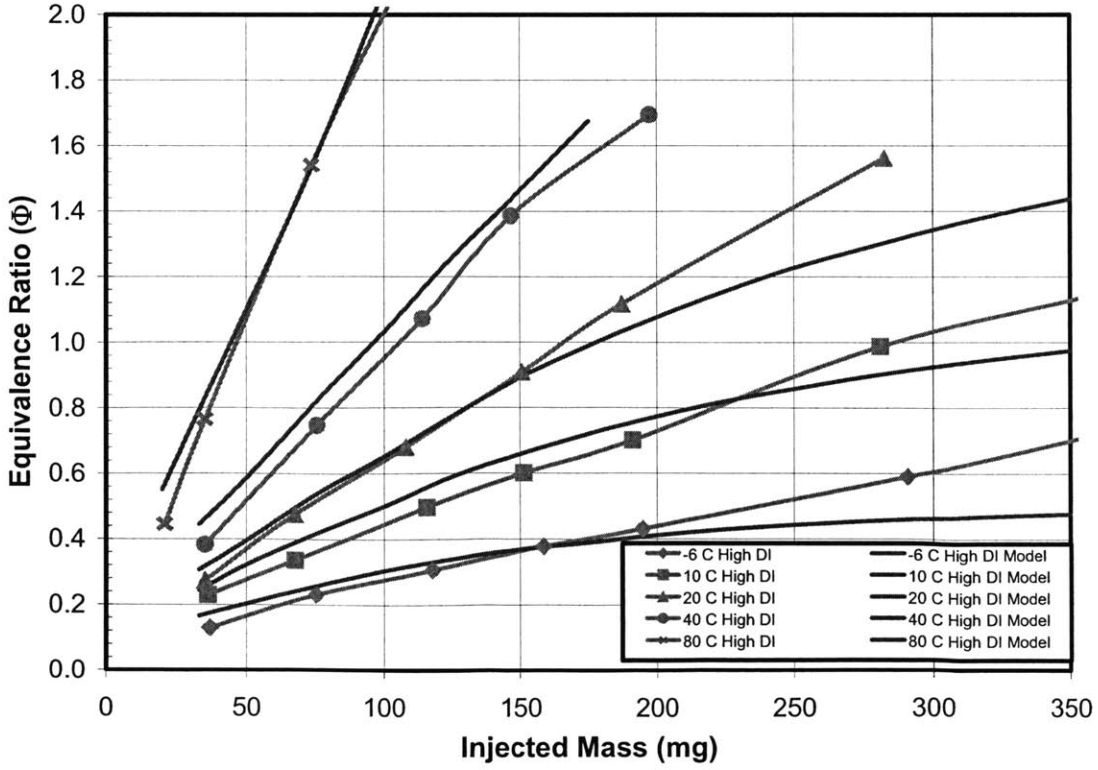

Figure 5.11 – Comparison of Test Data vs. Model

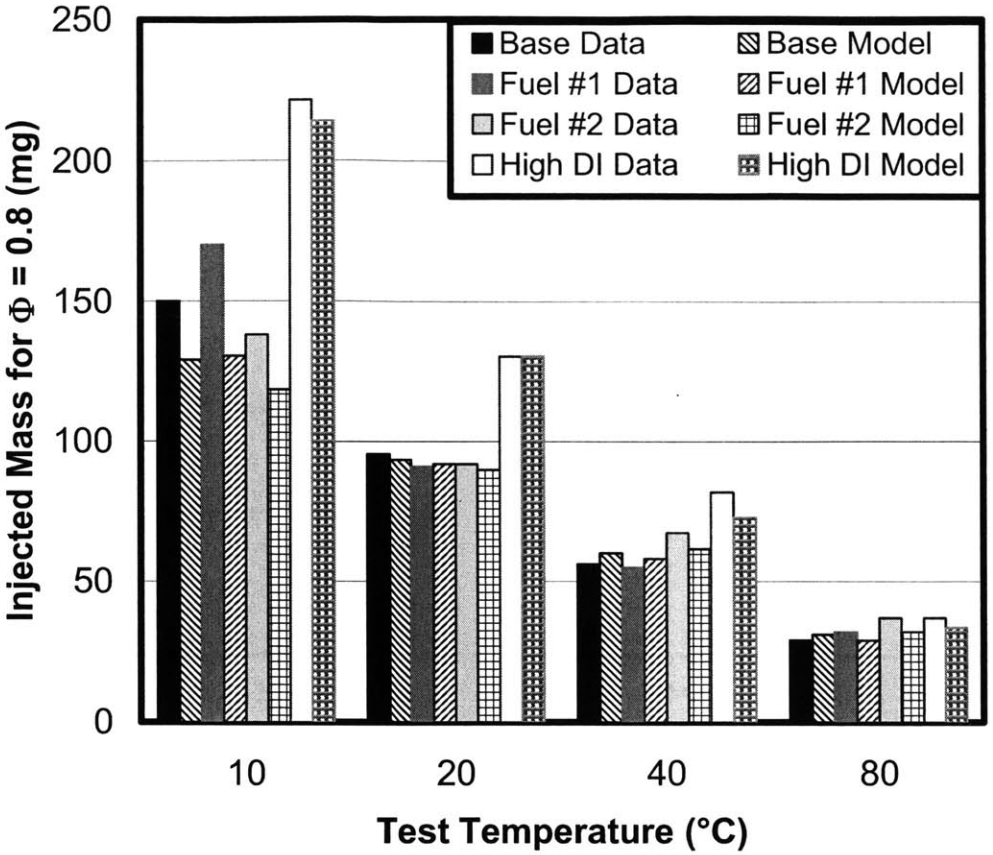

Chapter 6

SUMMARY & CONCLUSIONS

6.1 Conclusions

- Subtle differences in fuel volatility can produce significant differences in first cycle fuel delivery. With an adverse mixture preparation environment, limited energy is available to vaporize the liquid fuel in the intake port. The evaporative characteristics of the fuel therefore become critical to first cycle fuel delivery.
- First cycle fuel delivery can be correlated to points on the industry-standard ASTM distillation curve. At test temperatures of -6°C, 10°C, 20°C, and 40°C, the required injected mass to achieve an in-cylinder equivalence ratio (Φ) of 0.8 is proportional to T20, T30, T40, and T50, respectively.
- No clear correlation was established between fuel properties and fuel delivery at 80°C ECT. However, overfueling due to a conservative cranking strategy would be small on a mass basis, since the fuel delivery fraction is high.
- Increased fuel temperature during cold starts can improve first cycle fuel delivery as much as 30% at sub-freezing temperatures. Thus, pre-heating the fuel before injection could be a potential strategy for reducing cold start HC emissions.
- Relatively simple models for fuel composition and fuel delivery can capture most of the effects of fuel and temperature on first cycle fuel delivery. However, the model is only sensitive enough to capture the effects of fuels with substantially different distillation properties.

6.2 Direction of Future Work

- Further insight into first cycle fuel delivery could be obtained by analyzing the trapped air-fuel mixture with a gas chromatograph. This would verify which fuel components are actually vaporizing and entering the combustible mixture.
- With in-vehicle measuring capability, fuel properties could be incorporated into a production cold start strategy. Delphi is currently experimenting with an in-tank DI sensor [14], which

has been shown to have reasonable accuracy. A future study could investigate the use of this instrument to adjust first cycle fueling in response to fuel changes.

- Numerous strategies to reduce cold start HC emissions have been proposed, including the use of variable valve timing, charge motion control, and higher cranking speeds. In any study investigating one or more of these techniques, the sensitivity to fuel properties should be determined. An ideal fuel delivery technology would diminish the differences between fuels as much as possible.

REFERENCES

[1] Stanglmaier, R.H., Hall, M.J., Matthews, R.D., "In-Cylinder Fuel Transport During the First Cranking Cycles in a Port-Injected 4-Valve Engine," SAE Paper 970043, 1997.

[2] Takeda, K., Yaegashi, T., Sekiguchi, K., Saito, K., Imatake, N., "Mixture Preparation and HC Emissions of a 4-Valve Engine During Cold Starting and Warm-up," SAE Paper 950074, 1995.

[3] Morishima, R., Asai, K., "Mixture Strength at Cranking Cycles of Gasoline Engine Starting," SAE Paper 920235, 1995.

[4] Tomita, M., Okada, M., Katayama, H., Nakada, M., "Effect of Gasoline Quality on Throttle Response of Engines During Warm-Up," SAE Paper 900163, 1990.

[5] Coordinating Research Council, "1995-1997 CRC Study of Fuel Volatility Effects on Cold-Start and Warmup Driveability with Hydrocarbon, MTBE, and Ethanol Gasolines: Phase 4, Cold Temperature," CRC-605, 1998.

[6] Barker, D.A., Gibbs, L.M., Steinke, E.D., "The Development and Proposed Implementation of the ASTM Driveability Index for Motor Gasoline," SAE Paper 881668, 1988.

[7] Kaiser, E.W., Siegl, W.O., Baidas, L.M., Lawson, G.P., Cramer, C.F., Dobbins, K.L., Roth, P.W., Smokovitz, M., "Time-Resolved Measurement of Speciated Hydrocarbon Emissions During Cold Start of a Spark-Ignited Engine," SAE Paper 940963, 1994.

[8] Shibata, G., Omata, T., Isoda, T., Hosono, K., Nakamura, K., Tsuneishi, J., Kawano, H., "The Development of Driveability Index and the Effects of Gasoline Volatility on Engine Performance," SAE Paper 952521, 1995.

[9] Oda, K., Hosono, K., Isoda, T., Aihara, H., Kojima, K., Shibata, G. "Effect of Gasoline Composition on Engine Performance," SAE Paper 930375, 1993.

[10] Klein, D., Cheng, W.K., "Spark Ignition Engine Hydrocarbon Emissions Behaviors in Stopping and Restarting," SAE Paper 2002-01-2804, 2002.

[11] Castaing, B.M., Cowart, J.S., Cheng, W.K. "Fuel Metering Effects on Hydrocarbon Emissions and Engine Stability During Cranking and Start-Up in a Port Fuel Injected Spark Ignition Engine," SAE Paper 2000-01-2836, 2000.

[12] Santoso, H., "Mixture Preparation, Combustion, and Hydrocarbon Emissions at Different Cranking Speeds," MIT Press, Cambridge, 2002.

[13] Meyer, R., Heywood, J.B., "Evaporation of In-Cylinder Liquid Fuel Droplets in an SI Engine: A Diagnostic-Based Modeling Study," SAE Paper 1999-01-0567, 1999.

[14] Lambert, D.K., Harrington, C.R., Kerr, R., Lee, H.S., Lin, Y., Wang, D.Y., Wang, S.C., "Fuel Driveability Index Sensor," SAE Paper 2003-01-3238, 2003.

[15] Ikas, A.G., "Mixture Preparation Model for a Port Fuel Injected Spark Ignition Engine During the First Cycle of Cranking," MIT Press, Cambridge, 2001.

[16] Chen, K.C., DeWitte, K., Cheng, W.K., "A Species-Based Multi-Component Volatility Model for Gasoline," SAE Paper 941877, 1994.

[17] Santoso, H., Cheng, W.K., "Mixture Preparation and Hydrocarbon Emissions Behaviors in the First Cycle of SI Engine Cranking," SAE Paper 2002-01-2805, 2002.